Interpretation of gamma-ray burst X-ray and optical afterglow emission

From the central engine to the circumburst interaction

Liang Li

Academic dissertation for the Degree of Doctor of Philosophy in Theoretical Physics at Stockholm University to be publicly defended on Friday 9 February 2018 at 10.00 in sal FA32, AlbaNova universitetscentrum, Roslagstullsbacken 21.

Abstract

Gamma-ray bursts are the largest electromagnetic explosions known to happen in the Universe and are associated with the collapse of stellar progenitors into blackholes. After an energetic prompt emission phase, lasting typically less than a minute and emitted in the gamma-rays, a long-lived afterglow phase starts. During this phase strong emission is observed at longer wavelengths, e.g., in the X-ray and optical bands. This phase can last several weeks and carries important information about the energetics and structure of the burst as well as about the circumburst medium (CBM) and its density profile. The standard afterglow model includes a single emission component which comes from synchrotron emission in a blast wave moving into the CBM. Additional factors that could give observable features include prolonged energy injection from the central engine, effects of the jet geometry, and viewing angle effects, which thus constitute an extended standard model.

In this thesis, I study the afterglow emission in a global approach by analysing large samples of bursts in search for general trends and characteristics. In paper I, I compare the light curves in the X-rays and in the optical bands in a sample of 87 bursts. I find that 62% are consistent with the standard afterglow model. Among these, only 9 cases have a pure single power law flux decay in all bands, and are therefore fully described by the model within the observed time window. Including the additional factors described above, I find that 91% are consistent with the extended standard model. An interesting finding is that in nearly half of all cases the plateau phase (energy injection phase) changes directly into the jet decay phase. In paper II, I study the afterglow by analysing the temporal evolution of color indices (CI), defined as the magnitude difference between two filters. They can be used to study the energy spectrum with a good temporal resolution, even when high-resolution spectra are not available. I find that a majority of the CI do not vary with time, which means that the spectral slope does not change, even between different emission episodes. For the other cases, the variation is found to occur during limited periods. We suggest that they are due to the cooling frequency passing over the observed filter bands and, in other cases, due to the emergence of the underlying supernova emission. In paper III, I study the energetics of the GRBs that can be inferred from the afterglow observations. Using this information I analyse the limits it sets on what the central engine can be, if it is a magnetar or a spinning black hole. Assuming that the magnetar energy is emitted isotropically, I find that most bursts are consistent with a BH central engine and only around 20% are consistent with a magnetar central engine. As a consistency check, we derive the rotational energy and the spin period of the blackhole sample and the initial spin period and surface polar cap magnetic field for the magnetar sample and find them to be consistent to the expected values. We find that 4 of 5 of the short burst belong to the magnetar sample which supports the hypothesis that short GRB come from neutron star mergers.

Keywords: *gamma-ray bursts, central engine, afterglow.*

Stockholm 2018
http://urn.kb.se/resolve?urn=urn:nbn:se:su:diva-150386

ISBN 978-91-7797-118-4
ISBN 978-91-7797-119-1

Department of Physics

Stockholm University, 106 91 Stockholm

INTERPRETATION OF GAMMA-RAY BURST X-RAY AND OPTICAL AFTERGLOW EMISSION

Liang Li

Stockholm
University

Interpretation of gamma-ray burst X-ray and optical afterglow emission

From the central engine to the circumburst interaction

Liang Li

ISBN print 978-91-7797-118-4
ISBN PDF 978-91-7797-119-1

Cover illustration: Colour index variations in the afterglow of GRBs. The ratios of variable colour indices associated to a given phenomenon to the total number of variable colour indices in each time interval.

Printed in Sweden by Universitetsservice US-AB, Stockholm 2018
Distributor: Department of Physics, Stockholm University

Abstract

Gamma-ray bursts are the largest electromagnetic explosions known to happen in the Universe and are associated with the collapse of stellar progenitors into blackholes. After an energetic prompt emission phase, lasting typically less than a minute and emitted in the gamma-rays, a long-lived afterglow phase starts. During this phase strong emission is observed at longer wavelengths, e.g., in the X-ray and optical bands. This phase can last several weeks and carries important information about the energetics and structure of the burst as well as about the circumburst medium (CBM) and its density profile. The standard afterglow model includes a single emission component which comes from synchrotron emission in a blast wave moving into the CBM. Additional factors that could give observable features include prolonged energy injection from the central engine, effects of the jet geometry, and viewing angle effects, which thus constitute an extended standard model.

In this thesis, I study the afterglow emission in a global approach by analysing large samples of bursts in search for general trends and characteristics. In paper I, I compare the light curves in the X-rays and in the optical bands in a sample of 87 bursts. I find that 62% are consistent with the standard afterglow model. Among these, only 9 cases have a pure single power law flux decay in all bands, and are therefore fully described by the model within the observed time window. Including the additional factors described above, I find that 91% are consistent with the extended standard model. An interesting finding is that in nearly half of all cases the plateau phase (energy injection phase) changes directly into the jet decay phase. In paper II, I study the afterglow by analysing the temporal evolution of color indices (CI), defined as the magnitude difference between two filters. They can be used to study the energy spectrum with a good temporal resolution, even when high-resolution spectra are not available. I find that a majority of the CI do not vary with time, which means that the spectral slope does not change, even between different emission episodes. For the other cases, the variation is found to occur during limited periods. We suggest that they are due to the cooling frequency passing over the observed filter bands and, in other cases, due to the emergence of the underlying supernova emission. In paper III, I study the energetics of the GRBs that can be inferred from the afterglow observations. Using this information I analyse the limits it sets on what the central engine can be, if it is a magnetar or a spinning black

hole. Assuming that the magnetar energy is emitted isotropically, I find that most bursts are consistent with a BH central engine and only around 20% are consistent with a magnetar central engine. As a consistency check, we derive the rotational energy and the spin period of the blackhole sample and the initial spin period and surface polar cap magnetic field for the magnetar sample and find them to be consistent to the expected values. We find that 4 of 5 of the short burst belong to the magnetar sample which supports the hypothesis that short GRB come from neutron star mergers.

This thesis is dedicated to my dearest daughter and my family...

List of Papers

The following papers, referred to in the text by their Roman numerals, are included in this thesis.

PAPER I: **A Correlated Study of Optical and X-ray Afterglows of GRBs**
Liang Li; Xue-Feng Wu; Yong-Feng Huang; Xiang-Gao Wang; Qing-Wen Tang; Yun-Feng Liang; Bin-Bin Zhang; Yu Wang; Jin-Jun Geng; En-Wei Liang; Jian-Yan Wei; Bing Zhang; Felix Ryde, The Astrophysical Journal, 805, 13L (2015).
DOI:10.1088/0004-637X/805/1/13

PAPER II: **A Large Catalog of Multi-wavelength GRB Afterglows I: Colors Evolution And Its Physical Implication**
Liang Li, Yu Wang, Lang Shao, Xue-Feng Wu, Yong-Feng Huang, Bing Zhang, Felix Ryde, and Hoi-Fung Yu, The Astrophysical Journal Supplement Series, in press (2017).
DOI: 2017arXiv171203704

PAPER III: **Constraining the Type of Central Engine of GRBs with *Swift* data**
Liang Li, Xue-Feng Wu, Wei-Hua Lei, Zi-Gao Dai, En-Wei Liang and Felix Ryde, The Astrophysical Journal Supplement Series, submitted (2017).
DOI: 2017arXiv171209390

List of publications not included in the thesis

1: **A Search for Fermi Bursts Associated with Supernovae and Their Frequency of Occurrence**
Kovacevic, M.; Izzo, L.; Wang, Y.; Muccino, M.; Della Valle, M.; Amati, L.; Barbarino, C.; Enderli, M.; Pisani, G. B.; **Li, L.**, Astronomy and Astrophysics, 569, A108 (2014).
DOI: 10.1051/0004-6361/201424700

2: **Revisiting the Emission from Relativistic Blast Waves in a Density-jump Medium**
Geng, J. J.; Wu, X. F.; **Li, Liang**; Huang, Y. F.; Dai, Z. G., The Astrophysical Journal, 792, 31G (2014).
DOI:10.1088/0004-637X/792/1/31

3: **How Bad or Good Are the External Forward Shock Afterglow Models of Gamma-Ray Bursts?**
Wang, Xiang-Gao; Zhang, Bing; Liang, En-Wei; Gao, He; **Li, Liang**; Deng, Can-Min; Qin, Song-Mei; Tang, Qing-Wen; Kann, D. Alexander; Ryde, Felix; Kumar, Pawan, The Astrophysical Journal Supplement Series, 219, 9W (2015).
DOI:10.1088/0067-0049/219/1/9

4: **Imprints of Electron-Positron Winds on the Multiwavelength Afterglows of Gamma-ray Bursts**
Geng, J. J.; Wu, X. F.; Huang, Y. F.; **Li, L.**; Dai, Z. G., The Astrophysical Journal, 825, 107G (2016).
DOI:10.3847/0004-637X/825/2/107

5: **X-ray Flares in Early Gamma-ray Burst Afterglow**
Ruffini, R.; Wang, Y.; Aimuratov, Y.; Becerra, L.; Bianco, C. L.; Karlica, M.; Kovacevic, M.; **Li, L.**; Melon Fuksman, J. D.; Moradi, R.; and 8 coauthors, The Astrophysical Journal, in press, 2017arXiv170403821R (2017).
DOI: 2017arXiv170403821R

6: **Five *Fermi* collaboration published papers are not listed.**

Reprints were made with permission from the publishers.

Author's contribution

PAPER I

I headed the project which involves the study of the correlation between X-ray and optical afterglow with a break feature in the light curve using a large sample of GRBs. I was the main responsible for the data analysis, writing, and coordination between coauthors.

PAPER II

I headed the project which involves a systematic statistical analysis of the temporal evolution of color indices and a study of the physical interpretations of various types of variation of the color indices using a large sample of GRBs. I was the main responsible for the data analysis, writing, and coordination between coauthors.

PAPER III

I headed the project which involves a systematic statistical analysis of the *Swift*/XRT data to evaluate the possibility of a black hole being the central engine of GRBs. I was the main responsible for the data analysis, writing, and coordination between coauthors.

Contents

Abstract iv

List of Papers ix

List of publications not included in the thesis xi

Author's contribution xiii

List of Figures xvii

List of Tables xix

Acknowledgements xxi

1 Introduction 23
- 1.1 Basic observational properties of GRBs 23
- 1.2 The classical GRB fireball model 27
- 1.3 Thesis outline 28

2 The Fireball and the Afterglow Emission 29
- 2.1 The central engine 29
  - 2.1.1 Black hole central engine 29
  - 2.1.2 Magnetar central engine 30
  - 2.1.3 Energy injection into the fireball 30
- 2.2 Early dynamical evolution of the fireball 31
- 2.3 Afterglow emission 33
  - 2.3.1 Synchrotron power and characteristic energy 34
  - 2.3.2 Cooling frequency 34
  - 2.3.3 The power-law distribution of electrons 34
  - 2.3.4 The spectrum and light curve of synchrotron radiation 36
- 2.4 Afterglow external shock models 39
  - 2.4.1 Interaction with the circumburst medium 39
  - 2.4.2 The standard afterglow model 40

2.4.3 Energy injection afterglow model 42
2.4.4 Jet-break afterglow model 43
2.4.5 Closure relations 45
2.4.6 Canonical light curve 46

3 Satellite and Instruments Used in the Thesis **51**
3.1 Swift observations 51
3.2 Magnitudes, colors, and photometric systems 52
3.3 Ground-based optical and near-IR observations, and GCN operating principle 53

4 Summary of My Works **55**
4.1 A Correlated Study of Optical and X-ray Afterglows of GRBs 55
4.1.1 Context and aim 55
4.1.2 Results and conclusions 55
4.2 A Large Catalog of Multi-wavelength GRB Afterglows I: Color Evolution and Its Physical Implication 57
4.2.1 Context and aim 57
4.2.2 Results 57
4.3 Constraining the Type of Central Engine of GRBs with *Swift* data 60
4.3.1 Context and motivation 61
4.3.2 Results and conclusions 61

5 Conclusions and Outlook **65**

Sammanfattning **lxvii**

References **lxix**

List of Figures

1.1 The locations of 2704 GRBs based on *BATSE* on board NASA's *CGRO* during the nine-year mission. Figure taken from NASA[1]. 24

1.2 Distribution of T_{90} durations of GRBs based on *BATSE* observations [2]. 24

1.3 The prompt emission light curve of 12 bright GRBs, recorded by *BATSE*, which display a tremendous amount of diversity[3]. 25

1.4 The observed spectrum of a GRB can be modelled by the Band function which is characterized by 4 parameters: normalization, low energy index α, high energy index β, and peak energy $E_{\rm peak}$. This figure shows a GRB (GRB 090820) νF_ν (=Energy^2 times photon flux) spectrum with a Band function fit [4]. 26

1.5 Schematic figure of the fireball model, illustrating the production of the 'prompt' and 'afterglow' emission. Figure taken from https://www.nasa.gov. 27

2.1 The evolution of the Lorenz factor according to the fireball model. The outflow accelerates up to the saturation radius, $r_{\rm s}$=ηr_0, after which it starts coasting. $r_{\rm ph}$ is the photospheric radius, and $r_{\rm is}$ and $r_{\rm es}$ are the internal shock and external shock radius, respectively [5] 33

2.2 Electron distribution and the effect of fast and slow cooling cases. The electron spectrum index changes before (solid lines) and after (dashed lines) the electron cooling. 35

2.3 Typical spectra expected from synchrotron emission in GRBs. Figure reproduced from [6]. 37

2.4 Typical light curves expected from synchrotron emission in GRBs. Figure reproduced from [6]. 38

2.5 *Swift* canonical X-ray light curve [7]. 47

2.6 Synthetic schematic light curve of multiple optical emission components based on a large sample statistic [8]. 48

3.1 Swift Instrumentation and Swift's three scientific instruments: BAT, XRT and UVOT. Figure taken from: NASA/Goddard Space Flight Center. 51

4.1 The power-law indices for the light-curve decay. The black solid line indicates where are the X-ray and optical temporal indices are equal and the red and blue solid line indicates where $\alpha_x = \alpha_o \pm 0.25$, which is expected for the standard forward shock model with ISM and wind-like environments. The red and blue dashed lines are $\alpha_x = \alpha_o \pm 0.5$, which is expected for the energy injection case in a ISM and a wind-like environment, see Paper I. 56
4.2 In general the CI do not vary with time, as shown by the temporal evolution of all CI for all bursts. The Silver sample is in grey, while each color represents a different combination of bands for the Golden sample. Two horizontal black lines are CI equal -1 and 1, respectively. See Paper II for details. 58
4.3 The panel presents the ratios of *variable* CI associated to a given phenomenon to the total number of *variable* CI in each time interval (see text for detailed explanations). Different colors represent different phenomena [Paper II]. 59
4.4 The SED of afterglow present a deviated single power-law spectral slope. The star points represent the Golden griz bands while the circular points represent the Silver UBVRI bands [Paper II]. 60
4.5 The $E_{X,iso}$ compared against the $E_{K,iso}(t_b)$ with their distributions (black solid-lines) and the best Gaussian fits (red solid-lines). Different colors of scatter data points represent different sub-samples (Gold, Silver and Bronze). Two dash-lines represent $E_{X,iso}$ and $E_{K,iso}(t_b)$ equal 2×10^{52} erg, respectively [Paper III]. 62
4.6 The luminosity injection index q compared to the rotation parameter $a_\bullet$. Different colors of the points represent different sub-samples, the black perpendicular line represent $a_\bullet$=0.1, and different color dash-area describe q with different distributions for different $a_\bullet$ values [see further details in Paper III]. 63
4.7 The inferred magnetar parameters, initial spin period P_0 versus surface polar cap magnetic field strength B_p, derived for the Bronze samples. The vertical solid line is the breakup spin-period for a neutron star [9] [Paper III]. 64

List of Tables

2.1 The Closure Relation of Afterglows in Gamma-ray Bursts . . 46

Acknowledgements

First, I would like to express my heartfelt thanks to my supervisor Professor Felix Ryde, and the Erasmus Mundus Joint Doctorate Program that provided this great opportunity for me to study Astrophysics. No words can express my gratitude to Felix. I am greatly indebted to Felix for his valuable and enlighten scientific guidance in completing my Ph.D. I deeply appreciate his tolerance, patience and encouragement to me, allow me to explore my interests in a wider field of research, and let me learn the meaning and purpose of doing research. Also, I still remember he supported a short term apartment to help me through the difficulties when I first came to Stockholm, and booked an English course to improve my English skills. Even he took me personally to apply for my bank account. Also thanks to his family for Christmas dinners in the dark winters. His excellent qualities have infected me deeply. I will never forget what he did to me. I deeply miss my family and thanks to their support, especially to my parents, my wife and my two year's old daughter. I have always felt very guilty about my daughter. I missed a lot of her growing up. I only spent little time together with my daughter after she was born. They are my strong spiritual support.

I would like to thank my early and current office colleagues: Shabnam providing me with a lot of the details and information I need to live in Stockholm and the Erasmus Mundus program, and also so many other help, such as bringing me to the Swedish immigration to take my first permit card, etc. Christoffer for so many kind help and very useful discussion on gamma-ray bursts; Merlin, Zeynep and Vlasta for their interesting chats on everyday life. Serena for her delightful chat on Chinese Gongfu movies.

I would also like to express my great thanks to Michael, Damien, Hüsne, David, Josefin for all their support. Michael for so beneficial and insightful discussions on the *Fermi* data analysis and my project, 3ML, Python, Jupyter, Rmfit tools, etc. I really improved a lot with his help. Damien for he spent so much time helping me improve my writing skills, and discuss with me some useful rules for doing research. Hüsne for good discussion on data analysis of GRB afterglows, also very thankful for her ask Damien to pick up me at the airport when I first come to Europe in Nice. David for providing so many beneficial suggestions and discussions on revising my papers and thesis. Josefin for her good astronomy courses and useful discussion on data analysis. I have

really learned very much from all of you.

I also would like to thank all friends at KTH and Stockholm University. Thanks to Moszi for very friendly and eager help, thanks to Maxime, Elena, Oscar, Magnus, Victor, Edvin, Björn, Fei, Rupal, Mette, Dennis, Francesca, Linda, Rakhee, Nirmal, Stefan,Theodor-Adrian, Filip, Sumana, Elisabeth, Christian, Bemgt, Mark, Christer, all of you. Also, the Swedish traditional Fika provide us a good time every week. I would also like to thank all my classmates and friends in the cycle IV of Erasmus Mundus program, the meetings in Nice were really very enthusiastic and unforgettable. Thanks Irina, Onelda, Gabriel, Sergey, Tais, Srivatsan, Olof, Clement, Milos.

I am deeply grateful to Pascal, Emmanuel, Gildas, Clement, Cinzia for their immense support for me to all administrative procedures of the Erasmus Mundus program and Petra, Mona, Åsa, Isa, Per-Erik, Fawad, Edvard, and Sten at Stockholm University during my Ph.D. study. I would also like to thank Stockholm University especially for financial support.

I am also thankful to Prof. Remo Ruffini and Shesheng Xue for providing me an opportunity to work with them, when I stayed in Pescara for six months mobility. Also, thanks to Yu, Yuanbin, Xiaofeng, Rahim, Marco, Federica and Cinzia for their help in Italy. Yu and I have forged a deep friendship during my Ph.D. years. We often discuss, learn from each other, and improve together.

I also want to take this opportunity to express my great thanks to Prof. Bing Zhang and Xuefeng Wu. I never forget all the help from Bing, for his useful teaching of GRB courses in China, and beneficial discussions on my projects, and that he wrote the recommendation letter for me on Chinese New Year's eve, and has given me a lot of encouragement. Xuefeng for immense support to me when I went back to China to visit Nanjing every summer.

Finally, I would like to express my deepest appreciation to all my colleagues, my Supervisor, KTH, Stockholm University and Erasmus Mundus program, for providing such a wonderful and remarkable for science research and all the necessary facilities.

1. Introduction

Gamma-ray bursts (GRBs) are extremely bright explosions and the most energetic electromagnetic events in the Universe[1]. They are flashes of gamma-rays typically lasting for a few seconds to dozens of seconds, produced by either the collapse of a stellar-mass star into black hole or by the merger of two compact stars (neutron star-neutron star or neutron star-black hole). The photon energies mainly lie within the range 0.01-100 MeV, and the observed photon flux is between 0.01-100 $cm^{-2}s^{-1}$.

1.1 Basic observational properties of GRBs

GRBs were first discovered by the *Vela* satellites in 1967 but were not made public before 1973 [10]. After that the studies of GRBs were still in a dark era (1967-1990). Since the *Compton Gamma Ray Observatory* (*CGRO*) was launched and started to work in 1991, the study of GRBs began to be more extensive. *CGRO* carried the Burst and Transient Source Experiment (*BATSE*, 30 keV-2 MeV) instrument, which was the first large experiment designed for the study of GRBs, and was operational for 9 successful years. GRBs are detected 1-2 times per day. GRBs are found to be isotropically distributed in the sky which is shown by the 2704 *BATSE* GRB (Fig. 1.1). This strongly indicates a cosmological origin. The duration is defined as T_{90} which is the time during which 5%-95% of the burst fluence is observed. GRBs T_{90} shows a bimodal distribution based on the observations from *BATSE* [2]: short-harder bursts (T_{90} <2s) vs. long-softer bursts (T_{90} >2s) (see Fig. 1.2). The hardness ratio (HR) for short bursts are found to be harder than long ones[2].

The progenitor of short bursts is considered to be two neutron stars that undergo a merger, and as such give rise to an observable gravitational wave signal [11]. Short GRBs usually can be found in old galaxies and are located in outskirt regions of the galaxy, while long bursts originate from the collapse of a massive star, and are found in young galaxies with star-forming regions. GRBs usually have complicated temporal features (see Fig.1.3), and have a

[1]Coalescence of massive black holes, produce even more energetic events. However, in such cases, the energy is mainly released as gravitation waves and not an electromagnetic radiation.

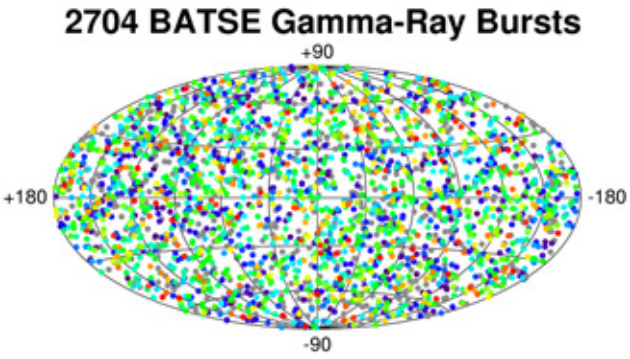

Figure 1.1: The locations of 2704 GRBs based on *BATSE* on board NASA's *CGRO* during the nine-year mission. Figure taken from NASA[1].

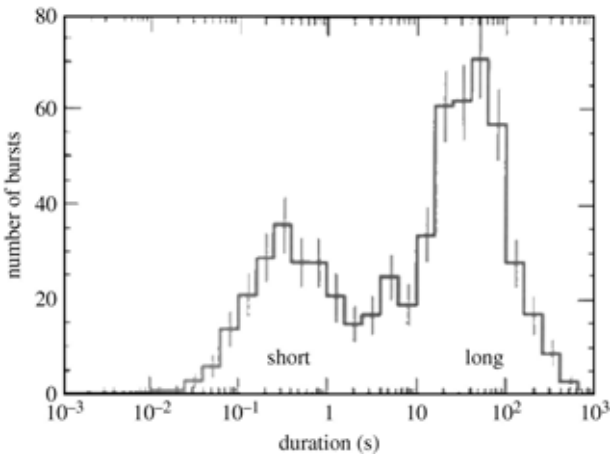

Figure 1.2: Distribution of T_{90} durations of GRBs based on *BATSE* observations [2].

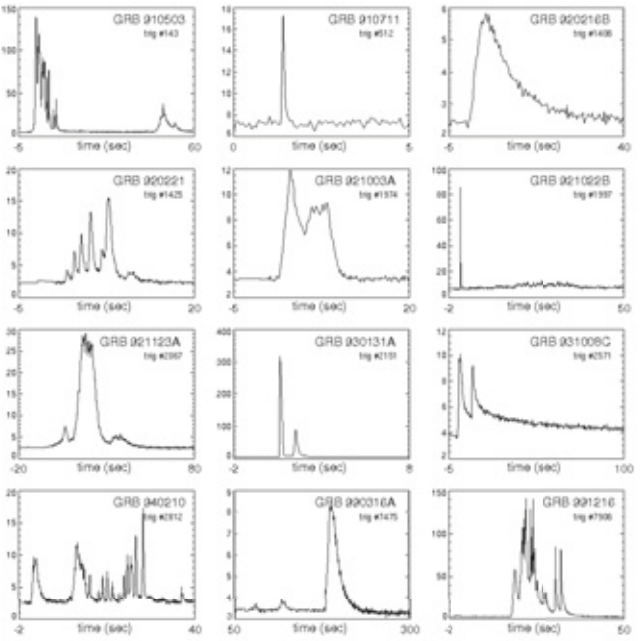

Figure 1.3: The prompt emission light curve of 12 bright GRBs, recorded by *BATSE*, which display a tremendous amount of diversity[3].

duration, usually ranging from milliseconds to hundred seconds, with a typical variability time scale of 0.1s-1s. The typical value of fluence is 10^{-10} to 10^{-8} J/m^2.

The observed GRB spectra show non-thermal features with a typically photon energy, ranging from few keV to several MeV, and most GRB spectra can be modelled by a Band et al. (1993) function [12], which is a smoothly joined broken power law with a low energy photon index $\alpha \sim$ -1 and a high energy photon index of $\beta \sim$ -2.1. The break energy $E_{\rm peak} \sim 250$ keV[13]. An example spectrum is shown in Fig. 1.4.

The debate on the origin of GRB at cosmological distances did not conclude until 1997, when afterglows were detected by *BeppoSAX* and the High Energy Transient Explorer (HETE) satellites (1997-2004). *BeppoSAX* discovered the broad-band afterglow of long GRBs. In 1997, the first afterglow observation was from GRB 970228 [14], which was detected as a fading X-ray source and also having an optical counterpart. The redshift of GRB 970228 was determined to be z=0.835. This confirmed that GRBs originate from cosmological distances. A breakthrough discovery in the *BeppoSAX* era was the GRB-SNe associations in some long bursts. The first GRB-SNe case occurred in 1998: GRB 980425 was followed by a detection of a bright supernova (SN

1998bw) [15], which showed that GRBs are associated with the death of massive stars. Furthermore, a significant break in the multiband optical afterglow light curve was found for GRB 990510, which indicates that GRB likely are jetted. The HETE-2 satellite provided quality afterglow positions and the clear

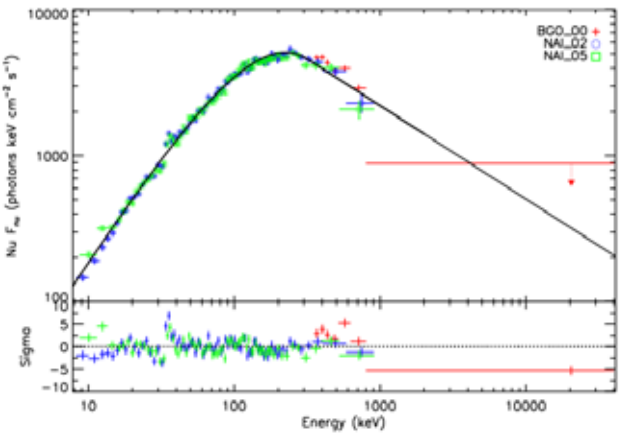

Figure 1.4: The observed spectrum of a GRB can be modelled by the Band function which is characterized by 4 parameters: normalization, low energy index α, high energy index β, and peak energy $E_{\rm peak}$. This figure shows a GRB (GRB 090820) νF_ν (=Energy^2 times photon flux) spectrum with a Band function fit [4].

detection of GRB 030329 in association with the supernova (SN 2003dh). The *International Gamma ray Astrophysics Laboratory* (*INTEGRAL*), launched by the European Space Agency (ESA) in 2002, also made many contributions, although GRB were not its main scientific goal. One important result of INTEGRAL was the detection of a low-energy GRB 031203, which was also confirmed to be associated with supernovae (SN 2003lw).

Later, further progress in observations were made by the *Swift* satellite. Since *Swift* was launched in 2004, GRB observations have entered a new era. *Swift* provides multi-wavelength (gamma rays, X-ray, ultraviolet and optical) observations and accurate localizations of the afterglow [16]. This has provided an opportunity to further understand the afterglow behaviors of GRBs. *Swift* discovered among other things, short GRB afterglows (GRBs 050509B, 050709, 050724). The high-z records were refreshed in the *Swift* era, with GRB 050904 (z=6.3); GRB 080913 (z=6.7); GRB 090423 (z=8.3), see further discussion in chapter 3. GRBs are observed currently by the *Fermi Gamma Ray Space Telescope*. *Fermi* was launched in 2008 and provides wider energy range (8 keV- 300 GeV). It carries two instruments: the Gamma ray burst monitor (GBM) [17] and the Large Area Telescope (LAT) [18]. *Fermi* has an unprecedented sensitivity, resolution and a large field of view. One of the

main goals is the continuous observation, in the gamma-ray band, of the whole celestial sphere (renewed observation every three hours). From GRB observations, several important conclusions have been made by *Fermi*, such as: an additional spectral component exists in some bursts, e.g., GRB090902B [19] and GRB090510 [20]; a delayed onset of the GeV afterglow emission and a long-lasting GeV afterglow are found in some GRBs (e.g. GRB 090510 [21]).

1.2 The classical GRB fireball model

The conventional model to explain GRBs evolution is the fireball model [22]. After the initial energy release at the central engine a relativistic and collimated outflow is emitted. The outflow is initially very hot and therefore denoted a fireball. GRBs have two main phases which are described by fireball model, the prompt emission and the afterglow emission (see Fig. 1.5).

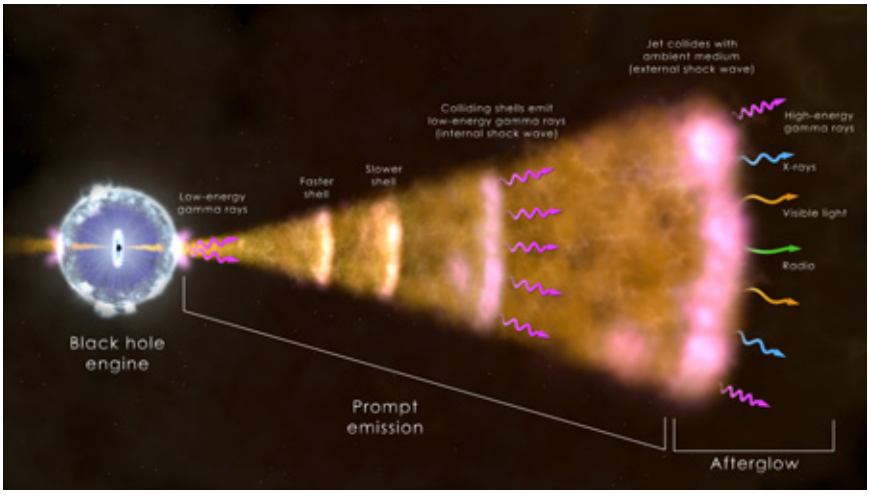

Figure 1.5: Schematic figure of the fireball model, illustrating the production of the 'prompt' and 'afterglow' emission. Figure taken from https://www.nasa.gov.

GRBs have a huge energy output with a typical order of magnitude of 10^{52} erg. The GRB energy can be estimated by observed quantities (flux of photons, giving the observed energy and the redshift, that is to say the distance). Through the light curve features, and light crossing arguments, the region of GRB emission can be constrained to $r = c\delta t \simeq 10^7$ cm, as an order of magnitude. Such a high energy in such a small region must produce a fireball.

Initially, the fireball has a large optical depth (τ). This is called the acceleration phase, and in which the energy is dominated by thermal energy. In the acceleration phase, the thermal energy is converted to kinetic energy of the flow. The Lorentz factor (Γ) increases with radius until Γ reaches its maximum value. At this time the thermal energy is approximately equal to the kinetic energy, and radius is called the saturation radius ($r_{\rm s}$). As the outflow continues to expands, the Lorentz factor (Γ) will stay constant. This phase is called the coasting phase or, equivalently, the mass dominated phase. More details are given in Chapter 2.

Before the fireball becomes optical-thin, the photon cannot escape. In the case the photons and electrons are fully thermalized, the spectral distribution of the photons can be described by a blackbody spectrum or a Planck function. The photospheric emission happens at τ=1 at radius $r_{\rm ph}$ when the thermal energy of the flow can be released. Within the internal shock model, the central engine emits many individual shells. If a shell with low-Γ is emitted preceding a later shell with high-Γ, the latter one will catch up the front one and collide. The shock created will accelerate electrons and cause synchrotron radiation, at a typical radius $r \sim 10^{14}$cm; At this time, the outflow still continues to move out and sweep up the circumburst medium (CMB). The circumburst medium interacts with the shell, and cause an external shock. This produces the multi-wavelength afterglow emission, seen in the X-ray, optical, and radio bands. The decay of the light curves and the Lorentz factor happens during the deceleration phase.

1.3 Thesis outline

In this thesis, I present statistical studies of large samples of the afterglow emission (X-ray and optical bands) used to investigate the conventional theoretical model. In paper I, I present a systematic statistical study of the relation between the X-ray and the optical afterglow to test various external shock models on a large sample. Paper II presents the time evolution of the color index in the afterglow emission based on another large sample to examine their physical origin. Paper III presents a systematic statistical study to investigate the GRB central engine, where we found that formation of a black hole could account for most of GRBs.

The thesis is structured in the following manner: in chapter 2, I present a discussion on the physics which is likely operating in GRBs. In chapter 3, I present the main instrument that are relevant to my works. In chapter 4, I present an introduction to my works with its backgrounds, motivations and main results. Finally, in chapter 5, I conclude my works and also present a future work perspectives.

2. The Fireball and the Afterglow Emission

2.1 The central engine

2.1.1 Black hole central engine

The collapse of the central parts of a massive star is thought to result in a rotating black hole. Conservation of angular momentum naturally causes its rotation to be significant. It is further assumed that an accretion disk is formed around it. If this disk has strong poloidal[1] magnetic fields, the energy and angular momentum of the rotating black hole can be extracted through the Blandford & Znajek (BZ, 1977) mechanism. Outside the event horizon, in a region called the ergosphere, an effect called frame-dragging twists the space-time which is dragged along in the direction of rotation. The poloidal magnetic fields are thus forced to rotate within the ergosphere which causes an extraction of spin energy from the black hole. Furthermore, the twisting of the magnetic field lines also play an important role in launching and collimating the jet forming a Poynting flux outflow.

The rotational energy of a black hole with angular momentum $J_\bullet$ is a fraction of the black hole mass $M_\bullet$, where $M_\odot$ is the solar mass [23].

$$E_{\rm rot} = f_{\rm rot}(a_\bullet)\left(\frac{M_\bullet}{M_\odot}\right)c^2{\rm erg} = 1.8\times10^{54} f_{\rm rot}(a_\bullet)\left(\frac{M_\bullet}{M_\odot}\right){\rm erg}, \tag{2.1}$$

where $a_\bullet = J_\bullet c/(GM_\bullet^2)$ is the black hole spin parameter, and

$$f_{\rm rot}(a_\bullet) = 1-\sqrt{(1+\sqrt{1-a_\bullet^2})/2}. \tag{2.2}$$

The total energy of GRBs is extracted from the central engine. Considering that the efficiency (η) cannot reach 100 percent, the total GRB energy ($E_{\rm tot}$) must less that the rotational energy of a black hole, therefore,

$$\eta E_{\rm rot} = f_{\rm b} E_{\rm tot}. \tag{2.3}$$

[1]The magnetic field lines are directed to the poles

where η is the efficiency of converting the spin energy to total energy of jet with the BZ mechanism, and f_b is the beaming factor of jet.

A part of jet energy is radiated in the form of prompt emission $E_{\gamma,\rm iso}$, and the remaining energy is kept in the form of a fireball kinetic energy $E_{\rm K,iso}$, in summary

$$E_{\rm tot} = E_{\gamma,\rm iso} + E_{\rm K,iso}. \tag{2.4}$$

Long-lasting activating of central energy can inject new energy to the external shock wave and refresh the external shock emission, thereby causing a plateau in the afterglow light curve. Therefore, the plateau phase can provide us with some information about the central engine.

2.1.2 Magnetar central engine

Alternatively, the collapse of the core does not need to result in the formation of a black hole immediately. Instead, a rapidly rotation proto-neutron star could be formed. The period would be ~ 1 ms and the surface magnetic field would be very strong ($B > 10^{15}$ G). Such an object is called a magnetar [24–32]. Polar jets are then driven by the extracted magnetic energy. The plateau phase in the afterglow can thus be explained by residual rotational and magnetic energy that is extracted after the main extraction event.

The maximum energy budget defined by the initial spin energy of the magnetar is that of the total rotation energy of the millisecond magnetar $E_{\rm rot} \sim 2\times10^{52}$ erg, but such a requirement does not exist for black holes. This fact provides a good clue to identify the candidate of GRB central engine.

The total rotation energy of the millisecond magnetar within this scenario is [33],

$$E_{\rm rot} = \frac{1}{2} I \Omega^2 \simeq 2\times10^{52}{\rm erg}{\rm M}_{1.4}{\rm R}_6^2{\rm P}_{0,-3}^{-2} \tag{2.5}$$

where I is the moment of inertia, $\Omega = 2\pi/P_0$ is the initial angular frequency of the neutron star, R is the stelar radius, P_0 is the initial spin period, and the convention $Q_x = 10^x Q$ is adopted in cgs units for all other parameters.

2.1.3 Energy injection into the fireball

Both the magnetar and black hole can produce a plateau in their afterglow light curve with an energy injection into the external shock.

The spindown luminosity of energy injection from a central engine is typically modeled to evolve with time as [34],

$$L(t) \simeq L_0 \left(\frac{t}{t_0}\right)^{-q} = \begin{cases} L_0 & ,t \ll \hat{\tau} \\ L_0 (t/\hat{\tau})^{-2} & ,t \gg \hat{\tau} \end{cases} \tag{2.6}$$

Here L_0 is the characteristic spin down luminosity, $\hat{\tau}$ is the initial spin-down timescale. The magnetar/black hole injection corresponds to q=0 for $t < \tau$ and q=2 for t$> \tau$). This evolution can be compared to observed afterglow light curves.

2.2 Early dynamical evolution of the fireball

The isotropic energy E has the typical value of 10^{52} erg and some GRBs even reach 10^{54} erg. Since the variability of the prompt emission light curve can be shorter than $\delta t_{\rm min} \sim 0.2$ ms, this restrict the radiation scale R_0, due to the light crossing argument

$$R_{\rm min} = c\delta t_{\rm min} \simeq R_0, \tag{2.7}$$

for a typical value of 10^7 cm. GRBs initially have such a great energy which is concentrate a upon such a small region, and its luminosity ($\sim 10^{51}$ erg s^{-1}) is much larger than the Eddington luminosity (with a typically value $\sim 10^{38}$ erg s^{-1}), which indicates that the radiation pressure is much larger than the self-gravitation, so there must be a fireball produced.

The optical depth τ is defined by,

$$\tau = \int n\sigma ds, \tag{2.8}$$

n is baryon number density, and σ is the Compton scattering cross-section. Most of the photons can not escape before the optical depth becomes $\tau <$1. During the optical thick phase ($\tau >$1), the fireball is fully thermalized and the photon distribution can be described by a blackbody spectrum. The energy density u (erg cm^{-3}) of photons with a blackbody spectrum is given by,

$$u = aT^4, \tag{2.9}$$

In the initial phase u$_0$=aT_0^4, where T_0 is the initial temperature of photons. In this phase, the baryon matter will be accelerated and the thermal energy will be converted into kinetic energy of the baryons.

We defined the dimensionless entropy η,

$$\eta = \frac{E}{\Gamma M_0 c^2} \tag{2.10}$$

E is the total energy, M_0 is the initial mass of the baryon (mainly protons), c is the speed of light, and Γ is the Lorentz factor which is given by,

$$\Gamma = \frac{1}{\sqrt{1-(\frac{v}{c})^2}} \tag{2.11}$$

v is the relative velocity between the two inertial systems, and c is the speed of light. Since the initial velocity of baryons are much less than c, the initial Lorentz factor Γ_0=1. The initial phase of the fireball $\eta_0 = E_0/M_0c^2$, here E_0 is the initial energy of photons.

Assuming the fireball to be spherical with a radius R, and V=$\frac{4}{3}\pi R^3$ is the volume, the total energy of the the plasma can be given by,

$$E_{\rm tot} = E_{\rm ph} + E_{\rm k} = u(r)V + \Gamma M_0 c^2 = \frac{4}{3}\pi R^3 a T^4 + \Gamma M_0 c^2, \tag{2.12}$$

The radiation energy of the photons of the fireball in the initial phase is,

$$E_0 = \frac{4}{3}\pi R_0^3 a T_0^4, \tag{2.13}$$

Using the typical value of parameters we can estimate the $T_0 \simeq 4.22 \times 10^{11}$ K. Here a=7.57 $\times$ 10^{-15} erg K^{-4} cm^{-3} is a radiation constant. Since the rest mass and energy of the baryons are negligible in the initial phase, we have E_{tot} $\simeq$ E_0.

The fireball evolution abide by the conservation of energy and entropy,

$$E_{\rm obs} \propto \Gamma(\mathrm{r})\mathrm{V}^{'}\mathrm{T}^{'}(\mathrm{r})^4 \propto \Gamma(\mathrm{r})\mathrm{r}^2\Gamma(\mathrm{r})\mathrm{r}_0\mathrm{T}^{'}(\mathrm{r})^4 = \text{constant}, \tag{2.14}$$

where $T^{'}$ (r) is the shell comoving temperature, and $V^{'}$ = $4\pi\mathrm{r}^2\mathrm{dr}^{'}$=$4\pi\mathrm{r}^2$ $\Gamma(\mathrm{r})\mathrm{r}_0$ is its comoving volume. The entropy in the comoving frame can be given by,

$$S^{'} = V^{'}(u^{'} + p^{'})/T^{'} \tag{2.15}$$

here $u^{'}$, $p^{'}$ are the internal energy density and pressure measured in the comoving frame. For photons, $p^{'} = u^{'}/3 \propto T^{'4}$.

$$S^{'} \propto V^{'}T^{'}(r)^3 \propto r^2\Gamma(r)r_0T^{'}(r)^3 = \text{constant}, \tag{2.16}$$

From Eq. (2.14) and Eq. (2.16), we can derive,

$$T^{'}(r) \propto r^{-1}, \tag{2.17}$$

$$\Gamma(r) \propto r, \tag{2.18}$$

$$V^{'} \propto r^3, \tag{2.19}$$

as the shell accelerates, $\Gamma(r)$ increases so the baryon kinetic energy $E_{\rm k}$=$\Gamma(r)Mc^2$ also increases, until it become comparable to the total fireball energy at Γ = $\Gamma_{\rm max} \simeq \eta$, at radius $r_s \sim \eta r_0$, see Fig. 2.1.

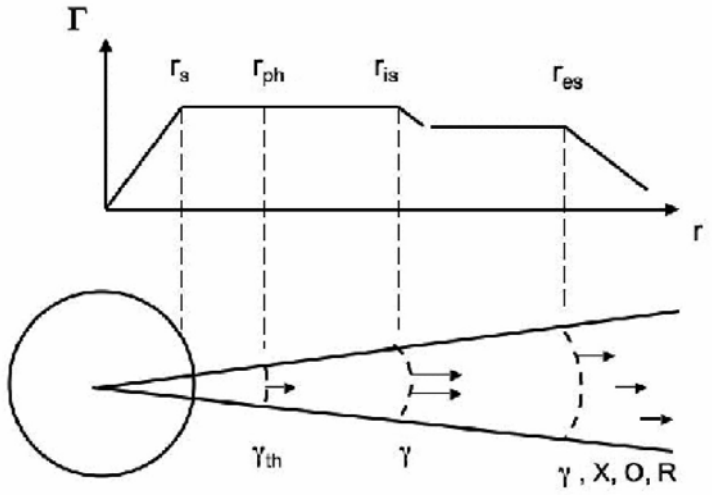

Figure 2.1: The evolution of the Lorenz factor according to the fireball model. The outflow accelerates up to the saturation radius, r_s=ηr_0, after which it starts coasting. r_{ph} is the photospheric radius, and r_{is} and r_{es} are the internal shock and external shock radius, respectively [5] .

Beyond the saturation radius r_s, most of the available energy is in kinetic form, and so the flow can no longer accelerate, and it coasts. The spatial evolution of the Lorentz factor is thus,

$$\Gamma(r) = \begin{cases} r/r_0, & r \leq r_s \\ \eta, & r \geq r_s \end{cases} \tag{2.20}$$

in the regime r $>$ r$_s$, since $\Gamma(r)$=constant, we can derive,

$$T^{'}(r) \propto r^{-2/3}, \tag{2.21}$$

$$\Gamma(r) = \eta, \tag{2.22}$$

$$V^{'} \propto r^2, \tag{2.23}$$

The observed temperature therefore evolves with radius as,

$$T_{\rm obs}(r) = \Gamma(r)T^{'}(r) = \begin{cases} T_0, & r \leq r_s \\ T_0 \times (r/r_s)^{-2/3}, & r \geq r_s \end{cases} \tag{2.24}$$

2.3 Afterglow emission

The current model to explain GRBs afterglow emission involves the external shock. After the internal shell collisions that produces part of the prompt emission, the bulk continues to move out and sweep up the circumburst medium

and will produce external shock (including a forward and a reverse shock). The shock accelerates electron, and produces magnetic fields, and therefore will emit synchrotron radiation. Likewise, since the observed GRB spectrum usually show a non-thermal feature, synchrotron emission has been extensively used to explain the observed GRB afterglow spectral.

2.3.1 Synchrotron power and characteristic energy

Synchrotron radiation is a kind of electromagnetic radiation in which the relativistic electrons deflection in the magnetic field produces emission along the tangent direction [35]. It has been widely applied in the field of high-energy astrophysics, since it is a very efficient emission mechanism which produces broad band and non thermal spectra. Many astrophysical objects have these properties, such as quasars, radio galaxy, etc.

The isotropic power radiation the emitted from a single electron is (the detailed derivation can be found in Rybicki & Lightman, 1979),

$$P(\gamma_e) = \frac{4}{3}\sigma_T c \gamma^2 \gamma_e^2 U_B \tag{2.25}$$

where σ_T is the Thomson cross section, γ_e is the electron Lorentz factor, U_B is the magnetic energy density, $U_B = \frac{B^2}{8\pi}$.

2.3.2 Cooling frequency

The cooling frequency (ν_c, γ_c is the corresponding electron Lorentz factor) is a critical value for synchrotron radiation. When relativistic electrons have $\gamma_e = \gamma_c$, the time scale of synchrotron radiation is equal that of dynamic the scale of the fireball. In other words, when the frequency of the electron is above the cooling frequency, the electron lose a significant fraction of their energy by synchrotron radiation, and all the electrons cool fast down to ν_c. This process is called fast cooling. On the other hand, when the frequency of the electron below ν_c, the electrons do not lose energy by synchrotron radiation. This process is called slow cooling.

2.3.3 The power-law distribution of electrons

After electrons are accelerated by the shock, it is typically assumed that the electrons have a power-law distribution $\frac{dN}{d\gamma_e} \propto \gamma_e^{-p}, \gamma_m < \gamma_e < \gamma_M$. γ_m and γ_M are the minimum and maximum Lorentz factors. In order to study the electron energy spectrum and its time dependence, it is useful to write down the energy

continuity equation. It is given by,

$$\frac{\partial(N(\gamma_e,t))}{\partial t}+\frac{\partial(\dot{\gamma}_e N(\gamma_e,t))}{\partial \gamma_e}=Q(\gamma_e,t), \tag{2.26}$$

where $Q(\gamma_e,t)$ is electron injection. For a steady state we have: $\frac{\partial(N(\gamma_e,t))}{\partial t}=0$, then,

$$\frac{\partial(\dot{\gamma}_e N(\gamma_e,t))}{\partial \gamma_e}=Q(\gamma_e,t). \tag{2.27}$$

We have two situations depicted in Figure 2.2:

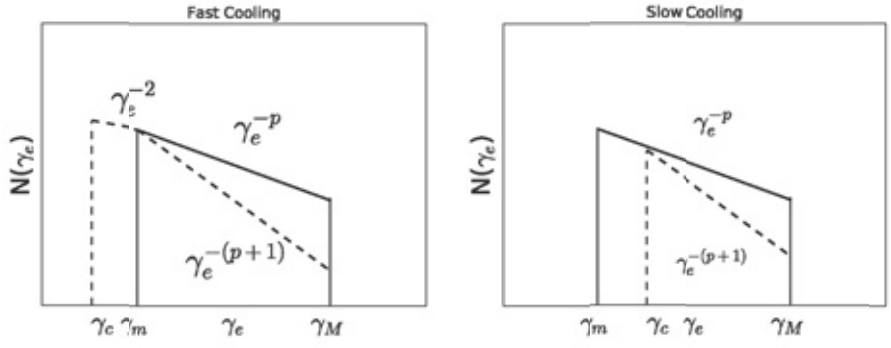

Figure 2.2: Electron distribution and the effect of fast and slow cooling cases. The electron spectrum index changes before (solid lines) and after (dashed lines) the electron cooling.

- Fast cooling ($\gamma_m > \gamma_c$): the frequency of all the electrons are above the cooling frequency. (i) For $\gamma_m > \gamma_e > \gamma_c$, since $Q(\gamma_e,t)$=0 and $\dot{\gamma}_e \propto \gamma_e^2$ according to equation (2.27), and we get $\frac{\partial(\gamma_e^2 N(\gamma_e,t))}{\partial \gamma_e}=0$, so we can derive $N(\gamma_e) \propto \gamma_e^{-2}$. (ii) For $\gamma_M > \gamma_e > \gamma_m$, since $Q(\gamma_e,t) \propto \gamma_e^{-p}$ and $\dot{\gamma}_e \propto \gamma_e^2$, so we get $\frac{\partial(\gamma_e^2 N(\gamma_e,t))}{\partial \gamma_e}=\gamma_e^{-p}$, after integration, we get $N(\gamma_e) \propto \gamma_e^{-(p+1)}$. Therefore,

$$\frac{dN}{d\gamma_e} \propto \begin{cases} \gamma_e^{-2}, & \gamma_m > \gamma_e > \gamma_c \\ \gamma_e^{-(p+1)}, & \gamma_M > \gamma_e > \gamma_m \end{cases} \tag{2.28}$$

- Slow cooling ($\gamma_c > \gamma_m$): the Lorentz factor cooling γ_c of electron lies between the minimum and the maximum Lorentz factor of the shocked fluid. (i) For $\gamma_M > \gamma_e > \gamma_c$, the electrons cool through synchrotron radiation, and $N(\gamma_e) \propto \gamma_e^{-(p+1)}$. (ii) For $\gamma_c > \gamma_e > \gamma_m$, the electrons do not

cool with synchrotron radiation, so they keep the original distributions: $N(\gamma_e) \propto \gamma_e^{-p}$. Therefore,

$$\frac{dN}{d\gamma_e} \propto \begin{cases} \gamma_e^{-p}, & \gamma_c > \gamma_e > \gamma_m \\ \gamma_e^{-(p+1)}, & \gamma_M > \gamma_e > \gamma_c \end{cases} \tag{2.29}$$

2.3.4 The spectrum and light curve of synchrotron radiation

According to Eq. (2.25), the radiation power for a single electron is given by: $P \propto \gamma_e^2$. Since the total number of electrons is $N(\gamma_e)d\gamma_e \propto \gamma_e^{-p}d\gamma_e$, we get the radiation power for total electron:

$$F_\nu d\nu \propto \gamma_e^2 \gamma_e^{-p} d\gamma_e. \tag{2.30}$$

On the other hand, the energy of photons related to synchrotron radiation of an electron, $\nu \propto \gamma_e^2$ gives $d\nu \propto \gamma_e d\gamma_e$, so we can derive $F_\nu \propto \nu^{-\frac{p-1}{2}}$. Similarly, applying this to different spectral regimes of synchrotron radiation, we get the radiation spectrum,

- Fast cooling:

$$F_\nu = F_{\nu,max} \begin{cases} (\nu_a/\nu_c)^{1/3}(\nu/\nu_a)^2, & (\nu_a > \nu) \\ (\nu/\nu_c)^{1/3}, & (\nu_c > \nu > \nu_a) \\ (\nu/\nu_c)^{-1/2}, & (\nu_m > \nu > \nu_c) \\ (\nu_m/\nu_c)^{1/2}(\nu/\nu_m)^{-p/2}, & (\nu > \nu_m) \end{cases} \tag{2.31}$$

- Slow cooling:

$$F_\nu = F_{\nu,max} \begin{cases} (\nu_a/\nu_m)^{1/3}(\nu/\nu_a)^2, & (\nu_a > \nu) \\ (\nu/\nu_m)^{1/3}, & (\nu_m > \nu > \nu_a) \\ (\nu/\nu_m)^{-(p-1)/2}, & (\nu_c > \nu > \nu_m) \\ (\nu_c/\nu_m)^{-(p-1)/2}(\nu/\nu_c)^{-p/2}. & (\nu > \nu_c) \end{cases} \tag{2.32}$$

Figure 2.3 shows typical spectra expected by the synchrotron emission for GRBs, different spectral regimes are separated by different frequencies (ν_a, ν_m, ν_c), and with different spectral indices. Here ν_a is the self-absorption frequency. The corresponding light curves are shown in Figure 2.4.

Also, the light curve can be derived as,

- High frequency ($\nu > \nu_0$):

$$F_\nu = \begin{cases} t^{1/6}, & (t_c > t) \\ t^{-1/4}, & (t_m > t > t_c) \\ t^{(2-3p)/4}, & (t_0 > t > t_m) \\ t^{(2-3p)/4}, & (t > t_0) \end{cases} \tag{2.33}$$

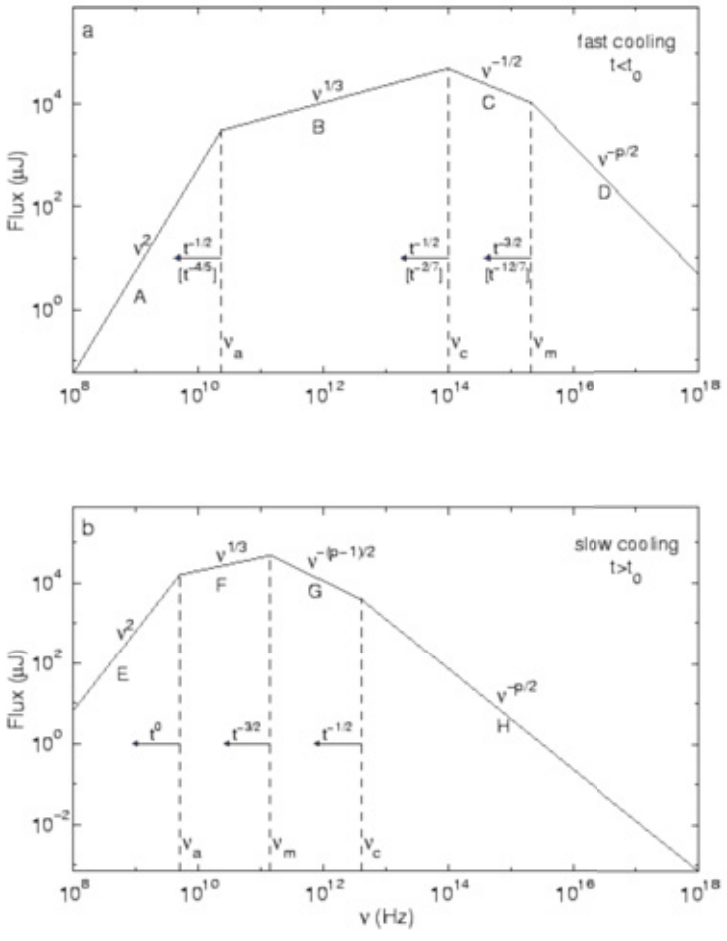

Figure 2.3: Typical spectra expected from synchrotron emission in GRBs. Figure reproduced from [6].

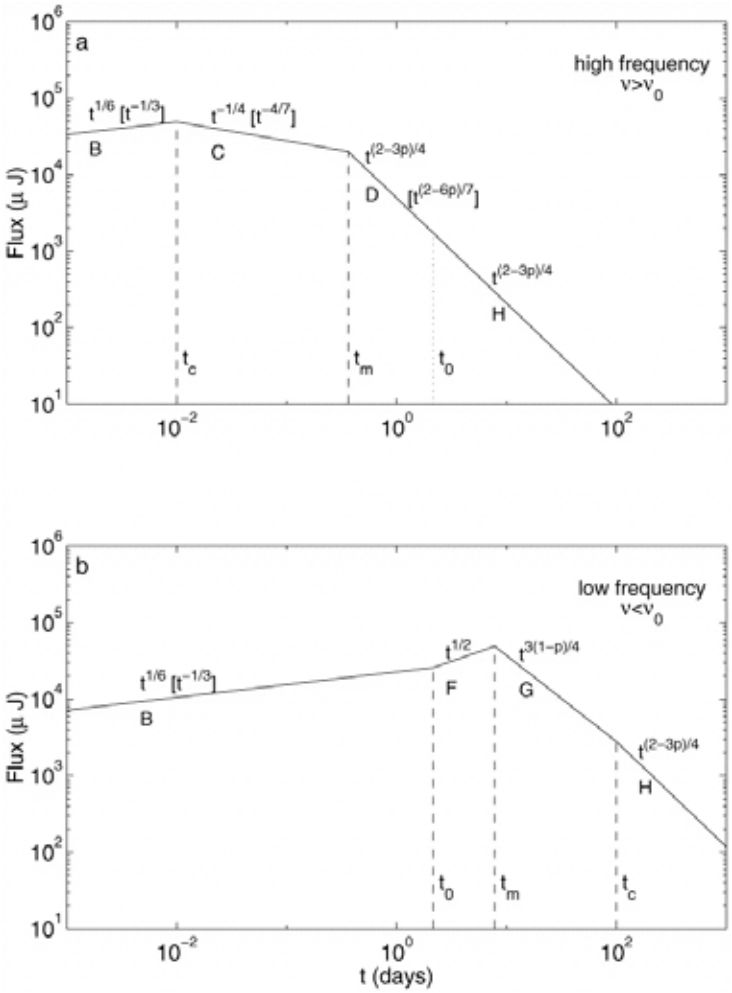

Figure 2.4: Typical light curves expected from synchrotron emission in GRBs. Figure reproduced from [6].

- Low frequency ($\nu < \nu_0$):

$$F_\nu = \begin{cases} t^{1/6}, & (t_0 > t) \\ t^{1/2}, & (t_m > t > t_0) \\ t^{3(1-p)/4}, & (t_c > t > t_m) \\ t^{(2-3p)/4}, & (t > t_c) \end{cases} \tag{2.34}$$

where ν_0 is the critical frequency, see Figure 2.4.

2.4 Afterglow external shock models

In the fireball model, two different shock models are used to explain both the initial burst of gamma-rays and the extended afterglow that is detected after the GRB: internal shocks and external shocks respectively. As mentioned in Section 2.3, the multi-bands afterglow emission is interpreted as synchrotron emission generated in a external forward shock as the blastwave interacts with the circum-burst medium [e.g., 6; 14; 36–39].

2.4.1 Interaction with the circumburst medium

The main component of the afterglow is created as the fireball interacts with the surrounding CMB. The relativistic blast wave theory provides a self-similar solution that is independent of details of the central engine. It thus naturally explains a simple power law evolution of the light curves across the electromagnetic spectrum.

This theory was first developed by Blandford & McKee [40] for AGN jets and later applied to GRB jets by Paczyński & Rhoads [41] and Mészáros & Rees [42]. Note that the latter papers were written before the discovery of the afterglow emission by *BeppoSAX* in 1997. Below, I derive the basic scalings for such a theory.

- Constant energy, constant density, ultrarelativistic, no energy injection

Consider the simplest case with constant energy, i.e., an adiabatic fireball with no energy injection, the shell is ultrarelativistic, and a constant circumburst medium density (ISM). Conservations of energy gives,

$$E = \frac{4\pi}{3} R^3 n m_p c^2 4\Gamma^2 = \text{constant}. \tag{2.35}$$

Therefore, one has $\Gamma^2 R^3$=constant, so

$$\Gamma \propto R^{-3/2}, R \propto \Gamma^{-2/3}. \tag{2.36}$$

The observed time reads

$$t \sim \frac{R}{2\Gamma^2} \propto R\Gamma^{-2} \propto \begin{cases} \Gamma^{-2/3}\Gamma^{-2} \propto \Gamma^{-8/3}, \\ RR^3 = R^4. \end{cases} \tag{2.37}$$

So one therefore has

$$\Gamma \propto R^{-3/2} \propto t^{-3/8}, R \propto t^{1/4}. \tag{2.38}$$

This corresponds to the self-simular power law decay beyond the radius $r_{\rm es}$ in Figure 2.1.

- Constant energy, but density stratification

We now consider a general density profile, i.e. a density stratification for which the number density can be written as

$$n = n_0 \left(\frac{R}{R_0}\right)^{-k}. \tag{2.39}$$

The energy conservation equation can be integrated over radius,

$$E = \int 4\pi R^2 n_0 \left(\frac{R}{R_0}\right)^{-k} m_p c^2 4\Gamma^2 dR = \text{constant}, \tag{2.40}$$

and we get $\Gamma^2 R^{3-k}$=constant. The observed time in this case

$$t \sim \frac{R}{2\Gamma^2} \propto R\Gamma^{-2} \propto \begin{cases} \Gamma^{\frac{2}{k-3}}\Gamma^{-2} \propto \Gamma^{\frac{8-2k}{k-3}}, \\ RR^{3-k} = R^{4-k}. \end{cases} \tag{2.41}$$

One gets

$$\Gamma \propto R^{\frac{k-3}{2}} \propto t^{\frac{k-3}{8-2k}}, R \propto t^{\frac{1}{4-k}}. \tag{2.42}$$

For a wind-like medium, $n \propto r^{-2}$, plugging in $k = 2$, one gets the scaling,

$$\Gamma \propto R^{-1/2} \propto t^{-1/4}, R \propto t^{1/2}. \tag{2.43}$$

2.4.2 The standard afterglow model

The simplest standard afterglow model has been extensively studied in past years [6]. Consider an 'ideal' dynamical evolution, with constant energy, constant density, an adiabatic fireball with no energy injection, which is the so-called 'the standard afterglow model'. A broadband spectrum (see Figure 2.3) and corresponding light-curves (see Figure 2.4) and relevant quantitative relationships have been studied by Sari et al. (1998). Observationally, studies largely confirmed the standard afterglow model in the pre-*Swift* era [e.g., 6; 14; 36; 38; 43]. Below the evolution of the spectra will be derived.

- Adiabatic ISM model

Considered the deceleration phase with constant energy and constant density (the simplest model), since $\Gamma \propto R^{-3/2} \propto t^{-3/8}$, $\gamma_m \propto \Gamma$, and $\gamma_c \propto \Gamma^{-1} t^{-1} B^{-2} \propto \Gamma^{-3} t^{-1}$ (see §2.4.1 for the ISM case) and $B \propto \Gamma$ [6], so one has

$$\nu_m \propto \Gamma \gamma_m^2 B \propto \Gamma^4 \propto t^{-3/2}, \tag{2.44}$$

$$\nu_c \propto \Gamma \gamma_c^2 B \propto \Gamma^{-1} t^{-2} B^{-3} \propto t^{-1/2}, \tag{2.45}$$

$$F_{\nu,max} \propto N_{tot} P_{\nu,max} \propto R^3 B \Gamma \propto R^3 \Gamma^2 \sim constant. \tag{2.46}$$

- Adiabatic wind model

The circum-burst medium of GRBs may not be a constant density medium but a more realistic wind-like medium. This has been studied by many authors, e.g., [44–47].

In this regime, since $\Gamma \propto R^{-1/2} \propto t^{-1/4}$, $R \propto t^{1/2}$, and $B \propto \Gamma n^{1/2} \propto t^{-1/4} R^{-1} \propto t^{-3/4}$ (see §2.4.1 for the wind case), so one has

$$\nu_m \propto \Gamma^3 B \propto t^{-3/2}, \tag{2.47}$$

$$\nu_c \propto \Gamma^{-1} t^{-2} B^{-3} \propto t^{1/2}, \tag{2.48}$$

$$F_{\nu,max} \propto RB\Gamma \propto t^{-1/2}. \tag{2.49}$$

The standard afterglow model was successful to explain the observed afterglow behavior in the pre-*Swift* era. Large amounts of observational data have been accumulated after the *Swift* launch. Some features such as the early X-ray afterglow has been challenging the conventional standard afterglow model, which clearly calls for additional assumptions to be made, e.g., prolonged energy injection, effect of the jet geometry, and viewing angle effects (e.g.,[34; 43; 48–54]). Findings based on these assumptions indicate that the afterglow emission is more complicated than that predicted by the simplest standard afterglow model (e.g. [55]), and further developments of models were made by various authors. Below we describe the main extension to the standard model.

2.4.3 Energy injection afterglow model

The 'ideal' standard afterglow model is based on many assumptions. The reality may not be so perfect. It is possible that the blastwave has energy continuously increasing with time. This is e.g. valid when a fireball is fed by a long-lasting Poynting-flux dominated wind (assuming the reverse shock does not exist or is extremely weak). Effectively, the energy in the wind can be added to the blastwave. This is the so-called 'energy injection model'.

Energy injection models have been extensively studied by many authors in recent years [34; 49; 50; 56]. These studied describe a long-lasting spinning-down central engine or piling up of flare material into the blastwave, and can be used to explain afterglow light curve that shows an initial plateau phase followed by a normal decay phase, corresponding to the standard model. The injected luminosity from central engine can be written,

$$L(t) = L_0 \left(\frac{t}{t_0}\right)^{-q}. \tag{2.50}$$

The total energy in the blastwave can be written as,

$$E_{\rm tot} = E_0 + E_{\rm inj} = E_0 + \int_0^t L(t)dt = E_0 + \frac{L_0 t_0^q}{1-q} t^{1-q}, \tag{2.51}$$

where $E_{\rm tot}$ is the total energy in the blastwave, E_0 is the initial energy in the blastwave, and $E_{\rm inj}$ is the injected energy into the blastwave from the long-lasting central engine. When $E_{\rm inj} \gg E_0$ the blastwave scaling becomes different, in this case, the total energy is given by,

$$E_{\rm tot} \sim E_{\rm inj} \propto t^{1-q}. \tag{2.52}$$

For the constant density (ISM) case (taking $t \propto R\Gamma^{-2}$), we have

$$\Gamma^2 R^3 \propto t^{1-q} \propto R^{1-q}\Gamma^{2(q-1)}. \tag{2.53}$$

Therefore, one finally has

$$\Gamma \propto R^{-\frac{2+q}{4-2q}} \propto t^{-\frac{2+q}{8}}, R \propto t^{\frac{2-q}{4}}. \tag{2.54}$$

For the wind-like case, since

$$\Gamma^2 R \propto t^{1-q} \propto R^{1-q}\Gamma^{2(q-1)}. \tag{2.55}$$

The scaling laws is finally given by

$$\Gamma \propto R^{\frac{q}{2q-4}} \propto t^{-\frac{q}{4}}, R \propto t^{\frac{2-q}{2}}. \tag{2.56}$$

- Adiabatic ISM energy injection model

For the adiabatic ISM energy injection model, according to Eqs. 2.54, we therefore get

$$\nu_m \propto \Gamma^2 \gamma_e B \propto \Gamma^4 \propto t^{-(2+q)/2}, \tag{2.57}$$

$$\nu_c \propto \Gamma^{-1} t^{-2} B^{-3} \propto t^{(q-2)/2}, \tag{2.58}$$

$$F_{\nu,max} \propto R^3 B \Gamma \propto t^{1-q}. \tag{2.59}$$

- Adiabatic wind-like energy injection model

Similarly, for the adiabatic wind-like energy injection model, according to Eqs. 2.56, which can be written as

$$\nu_m \propto \Gamma^3 B \propto t^{-(2+q)/2}, \tag{2.60}$$

$$\nu_c \propto \Gamma^{-1} t^{-2} B^{-3} \propto t^{(2-q)/2}, \tag{2.61}$$

$$F_{\nu,max} \propto RB\Gamma \propto t^{-q/2}. \tag{2.62}$$

2.4.4 Jet-break afterglow model

GRBs are very likely collimated [43; 51; 52; 57; 58], and a good fraction of GRBs have been observed with an afterglow steepening at a certain point. This can be interpreted as evidence of a jet break. There are two reasons for a steepening in the light curve decay slope: edge effect and sideway expansion.

- Edge effect

The jet opening angle θ_j is assumed not change throughout the edge effect.

For the adiabatic ISM case: the same dynamics, one has $\Gamma \propto R^{-3/2} \propto t^{-3/8}$, $\nu_m \propto t^{-3/2}$, and $\nu_c \propto t^{-1/2}$. Comparing with Eq. (2.46), the difference is

$$F_{\nu,max} \propto R^3 B \Gamma \frac{\theta_j^2}{(1/\Gamma)^2} \propto R^3 B \Gamma^3 \propto t^{-3/4}. \tag{2.63}$$

Since $B \propto \Gamma$, this indicates the light curve of all regimes steepen by a factor: $\Gamma^2 \propto t^{-3/4}$. For the adiabatic wind case: $\Gamma \propto R^{-1/2} \propto t^{-1/4}$, $\nu_m \propto t^{-3/2}$, and $\nu_c \propto t^{-1/2}$. Comparing to Eqs. (2.49), the difference is

$$F_{\nu,max} \propto RB\Gamma(\Gamma\theta_j)^2 \propto RB\Gamma^3 \propto t^{-1}. \tag{2.64}$$

Similarly, this implies a factor $\Gamma^2 \propto t^{-1/2}$ steeper for the jet case than the isotropic case.

Therefore, the change of temporal decay slope for the post jet break with a edge effect,

$$\alpha_2 = \begin{cases} \alpha_1 + 3/4, & (\text{ISM}) \\ \alpha_1 + 1/2, & (\text{Wind}) \end{cases} \tag{2.65}$$

Here α_1 and α_2 are the temporal slopes of pre- and post jet break, respectively.

- Sideways expansion

The jet opening angle θ_j could increase due to sideways expansion [51; 52]. Consider it with an expansion speed which may be even close to speed of light, for relativistic expansion [52], so

$$\theta_j = \theta_{j,0} + \frac{ct^{'}}{ct} \simeq \theta_{j,0} + \frac{1}{\Gamma}. \tag{2.66}$$

So when $\Gamma^{-1} > \theta_{j,0}$, one has $\theta_j \sim \Gamma^{-1}$.

For the ISM model [52],

$$\nu_m \propto \Gamma^4 \propto t^{-2}, \tag{2.67}$$

$$\nu_c \propto \Gamma^{-1} t^{-2} B^{-3} \propto t^0, \tag{2.68}$$

$$F_{\nu,max} \propto R^3 B \Gamma \propto R^3 \Gamma^2 \propto t^{-1}. \tag{2.69}$$

Therefore, the post jet-break afterglow behavior reads (consider slow cooling relevant)

$$F_\nu = \begin{cases} \nu^{1/3} t^{-1/3}, & (\nu_a < \nu < \nu_m) \\ \nu^{-(p-1)/2} t^{-p}, & (\nu_m < \nu < \nu_c) \\ \nu^{-p/2} t^{-p}, & (\nu > \nu_c) \end{cases} \tag{2.70}$$

So the decay slope is essentially defined by the electron spectral index $\alpha \propto t^{-p}$ for the X-ray and the optical bands. Since p with a typical value ~ -2.5, this suggest a sharper break than the edge effect model.

- Inferring jet opening angle from the jet break time

Within the framework of the uniform jet model, the jet opening angle can be inferred from the afterglow break time, with

$$\theta_j \simeq \frac{1}{\Gamma(t_j)}. \tag{2.71}$$

Since $R = 2c\Gamma^2 \frac{t}{1+z}$, so $E_{\rm K,iso}$ can be written as,

$$E_{\rm K,iso} = \frac{4\pi}{3} R^3 n m_p c^2 \Gamma^2 = \frac{32\pi}{3} \Gamma^8 \left(\frac{t}{1+z}\right)^3 n m_p c^5. \tag{2.72}$$

Therefore

$$\Gamma = \left(\frac{3E_{\rm K,iso}}{32\pi n m_p c^5}\right)^{1/8} t_j^{-3/8} (1+z)^{3/8}, \tag{2.73}$$

and therefore the jet opening angle is

$$\theta_j = \frac{1}{\Gamma} = \left(\frac{32\pi n m_p c^5}{3E_{\rm K,iso}}\right)^{1/8} t_j^{3/8} (1+z)^{-3/8}. \tag{2.74}$$

For the ISM model, since $\theta_j \propto t_j^{3/8}$ (since $\Gamma \propto t_j^{-3/8}$), one gets ([59]),

$$\theta_j = 0.06 \left(\frac{t_j}{1{\rm day}}\right)^{3/8} \left(\frac{1+z}{2}\right)^{-3/8} \left(\frac{E_{\gamma,iso}}{10^{53}{\rm ergs}^{-1}}\right)^{-1/8} \left(\frac{\eta_\gamma}{0.2}\right)^{1/8} \left(\frac{n}{0.1{\rm cm}^{-3}}\right)^{1/8}, \tag{2.75}$$

and,

$$f_{\rm b} = 1 - cos\theta_j \simeq (1/2)\theta_j^2, \tag{2.76}$$

where η_γ is an efficiency factor in γ-ray, and f_b is the beaming correction.

After we obtain a θ_j, the total energy with a beaming correction can be written by $E_\gamma = E_{\gamma,{\rm iso}} f_b = E_{\gamma,{\rm iso}}(1 - cos\theta_j)$.

2.4.5 Closure relations

The flux density F_ν can be written as

$$F_\nu = \nu^{-\beta} t^{-\alpha}, \tag{2.77}$$

where α and β are temporal and spectral indices, respectively. It is interesting to investigate the $\alpha - \beta$ relations in different spectral regimes. The relationship between temporal and spectral indices are denoted by closure relations [7; 60]. These can quickly assist to judge which afterglow model works.

We focus on the X-ray and optical emission, where synchrotron self-absorption is not important. So the spectral regimes which are above the self-absorption frequency (ν_a) are typically considered. The adiabatic ISM afterglow model together with the adiabatic wind afterglow model, the closure relations can be written as follows.

For fast cooling case:

$$\alpha = \begin{cases} \frac{\beta}{2}, & \nu_{\rm c} < \nu < \nu_{\rm m}({\rm ISM}), \\ \frac{1-\beta}{2}, & \nu_{\rm c} < \nu < \nu_{\rm m}({\rm Wind}), \\ \frac{3\beta-1}{2}, & \nu > \nu_{\rm m}({\rm ISM\ and\ Wind}), \end{cases} \tag{2.78}$$

Table 2.1: The Closure Relation of Afterglows in Gamma-ray Bursts [7]

		no injection		injection	
	β	α	$\alpha(\beta)$	α	$\alpha(\beta)$
ISM		slow cooling			
$\nu < \upsilon_m$	$-\frac{1}{3}$	$-\frac{1}{2}$	$\alpha = \frac{3\beta}{2}$	$\frac{5q-8}{6}$	$\alpha = (q-1) + \frac{(2+q)\beta}{2}$
$\upsilon_m < \nu < \upsilon_c$	$\frac{p-1}{2}$	$\frac{3(p-1)}{4}$	$\alpha = \frac{3\beta}{2}$	$\frac{(2p-6)+(p+3)q}{4}$	$\alpha = (q-1) + \frac{(2+q)\beta}{2}$
$\nu > \upsilon_c$	$\frac{p}{2}$	$\frac{3p-2}{4}$	$\alpha = \frac{3\beta-1}{2}$	$\frac{(2p-4)+(p+2)q}{4}$	$\alpha = \frac{q-2}{2} + \frac{(2+q)\beta}{2}$
ISM		fast cooling			
$\nu < \upsilon_c$	$-\frac{1}{3}$	$-\frac{1}{6}$	$\alpha = \frac{\beta}{2}$	$\frac{7q-8}{6}$	$\alpha = (q-1) + \frac{(2-q)\beta}{2}$
$\upsilon_c < \nu < \upsilon_m$	$\frac{1}{2}$	$\frac{1}{4}$	$\alpha = \frac{\beta}{2}$	$\frac{3q-2}{4}$	$\alpha = (q-1) + \frac{(2-q)\beta}{2}$
$\nu > \upsilon_m$	$\frac{p}{2}$	$\frac{3p-2}{4}$	$\alpha = \frac{3\beta-1}{2}$	$\frac{(2p-4)+(p+2)q}{4}$	$\alpha = \frac{q-2}{2} + \frac{(2+q)\beta}{2}$
Wind		slow cooling			
$\nu < \upsilon_m$	$-\frac{1}{3}$	0	$\alpha = \frac{3\beta+1}{2}$	$\frac{q-1}{3}$	$\alpha = \frac{q}{2} + \frac{(2+q)\beta}{2}$
$\upsilon_m < \nu < \upsilon_c$	$\frac{p-1}{2}$	$\frac{3p-1}{4}$	$\alpha = \frac{3\beta+1}{2}$	$\frac{(2p-2)+(p+1)q}{4}$	$\alpha = \frac{q}{2} + \frac{(2+q)\beta}{2}$
$\nu > \upsilon_c$	$\frac{p}{2}$	$\frac{3p-2}{4}$	$\alpha = \frac{3\beta-1}{2}$	$\frac{(2p-4)+(p+2)q}{4}$	$\alpha = \frac{q-2}{2} + \frac{(2+q)\beta}{2}$
Wind		fast cooling			
$\nu < \upsilon_c$	$-\frac{1}{3}$	$\frac{2}{3}$	$\alpha = \frac{1-\beta}{2}$	$\frac{1+q}{3}$	$\alpha = \frac{q}{2} - \frac{(2-q)\beta}{2}$
$\upsilon_c < \nu < \upsilon_m$	$\frac{1}{2}$	$\frac{1}{4}$	$\alpha = \frac{1-\beta}{2}$	$\frac{3q-2}{2}$	$\alpha = \frac{q}{2} - \frac{(2-q)\beta}{2}$
$\nu > \upsilon_m$	$\frac{p}{2}$	$\frac{3p-2}{4}$	$\alpha = \frac{3\beta-1}{2}$	$\frac{(2p-4)+(p+2)q}{4}$	$\alpha = \frac{q-2}{2} + \frac{(2+q)\beta}{2}$

For slow cooling case:

$$\alpha = \begin{cases} \frac{3\beta}{2}, & \nu_{\rm m} < \nu < \nu_{\rm c}({\rm ISM}), \\ \frac{3\beta+1}{2}, & \nu_{\rm m} < \nu < \nu_{\rm c}({\rm Wind}), \\ \frac{3\beta-1}{2}, & \nu > \nu_{\rm c}({\rm ISM\ and\ Wind}), \end{cases} \tag{2.79}$$

All the closure relations with the convention (2.77) are listed in Table 2.1 [7].

2.4.6 Canonical light curve

X-ray afterglow canonical light curve.

Based on the rich data accumulated from the *Swift* satellite, the statistical analysis shows that the X-ray canonical afterglow light curve has 5 components [7], which may have different physical origins, see Fig. 2.5.

- Phase I. Steep decay:

  Early steep decay is naturally considered as a tail of prompt emission of GRBs [61], with a very steep temporal decay slope (from t^{-3} to t^{-8}),

and a typical early observation time scale (dozens of seconds to hundred seconds).

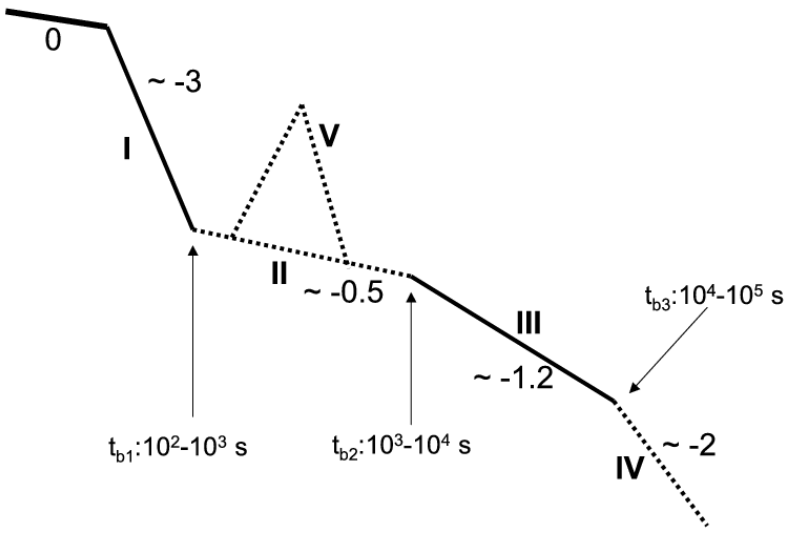

Figure 2.5: *Swift* canonical X-ray light curve [7].

- Phase II. Shallow decay phase (also called 'plateau' phase):

  After the steep decay, the light curve sometimes transitions to a shallow decay segment, with a typical temporal slope t^0 to t^{-1}, and a typical observation time scale (several 10^2 seconds to $\sim 10^4$ seconds). It usually is followed by a normal decay phase with $t^{-1.2}$, and occasionally followed by a very steep decay (t^{-3} to t^{-8}, e.g. GRB 070110[62]). It is usually interpreted with an internal origin, so-called 'internal plateau'.

- Phase III. Normal decay phase:

  The normal decay is expected in the standard afterglow model with a typical temporal slope $t^{-1.2}$ (the value is estimated by $t^{-(3p-2)/4}$ in the ISM medium, slow cooling, $\nu_m < \nu < \nu_c$, and assuming electron spectral index to have a typical value $p \sim 2.5$.).

- Phase IV. Post-jet break phase:

  Some GRBs have been observed with a late steep decay transition from the normal decay, which possibly is due to a jet break, with a typical

temporal decay slope t^2 or steeper and with a typical observed time scale $\sim 10^5$ seconds.

- Phase IV. X-ray flare:

  The flares are characterized by rapid rise and fall features, with many properties similar to the prompt emission. Therefore it is usually believed that these are due to late central engine activity.

Not all GRBs are observed to have all 5 components.

Optical afterglow canonical light curve.

Compared with the X-ray afterglows, the optical afterglows have more complicated light curves with up to eight emission components that could be explained by different physical origins [8; 63–70]. Based on the statistical results of large samples, a synthetic optical afterglow light curve [8] is presented in Li et al. (2012), see Fig. 2.6.

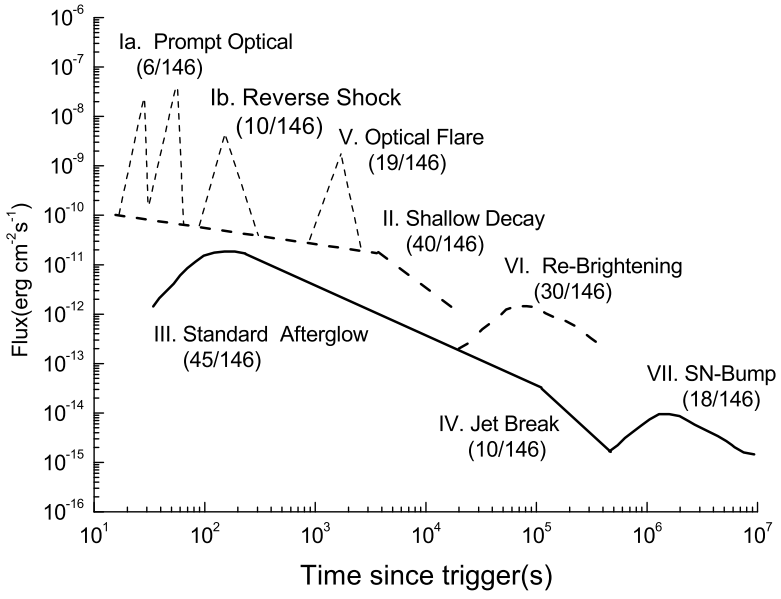

Figure 2.6: Synthetic schematic light curve of multiple optical emission components based on a large sample statistic [8].

- Ia: the prompt optical flares (Prompt-Optical); in the very early time of some bursts when the prompt GRB emission is still going on, a highly variable optical emission component may be observed (such as: GRB

041209A, 080319B). It has a rapid rise and fall features with the temporal slope, and with a observation time smaller than T_{90}.

- Ib: the early optical flares (Reverse-Shock); in a few cases, the early light curves have steep slopes, which likely indicate an early reverse shock emission component (such as: GRB 061126), with a typical temporal index $\alpha \sim 1.7$ and the peak time $t_{\rm p}$ of few hundreds of seconds.

- II: an early shallow-decay component (Energy-Injection); Similar to the X-ray afterglow, the optical afterglow light curve might show an initial shallow decay segment, which is likely due to energy injection from a long-lasting spinning-down central engine or piling up of flare materials into the blastwave ([8; 71]). They have a typical temporal index value $\alpha \sim 0.5$, and with a typical value of break time $t_{\rm b} \sim 10^4$ seconds.

- III: the standard afterglow component (Onset/Normal-Decay); the light curves sometimes have an early onset rising segment followed by a normal decay. In most of the cases, a lack of observation in the early time lead to only a single normal decay. Afterglow onsets are identified with an early smooth bump with a typical value of peak time $t_{\rm p}$ of several hundreds of seconds, coupled to the following normal decay with $\alpha \sim 1.2$.

- IV: the jet-break component (Jet-Break); the light curves break into a steeper decay. They are identified with $\alpha \sim 2.0$ or steeper ([7]) and a break time $\sim 10^5$ seconds.

- V: the late optical flares (Flare); the light curves have prompt-like flares during the afterglow phase when the prompt emission is turned off. They indicate the late-time activities of the central engine. The late optical flares are characterized by a very sharp temporal index α steeper than 2.

- VI: the late re-brightening bumps (Re-Bump); the late bumps would emerge at late times which is distinguished from the onset-bump of the early afterglow. Both are likely involved in the jet component that produces the re-brightening bump which seems to be on-axis and independent of the prompt emission jet component. They are described by a smooth bump around $t_{\rm p} \sim 10^5$ seconds.

- VII: the late supernova (SN) bumps (SN-Bump); in some cases, the optical transient light curves at late time show SN bump. They form a late smooth bump at $t_{\rm p} \sim 10^6$ seconds.

Similar to the X-ray, not all GRBs are observed to have all 8 components in the optical afterglow light curves.

3. Satellite and Instruments Used in the Thesis

3.1 Swift observations

The *Swift Gamma Ray Burst Mission* [16], was launched on November 20, 2004, specifically designed for observation of gamma-ray bursts and fast follow-up observations. It can observe in gamma ray, X-ray, ultraviolet and the visible bands. The satellite is in a low earth orbit, about 600 km in altitude with a cycle

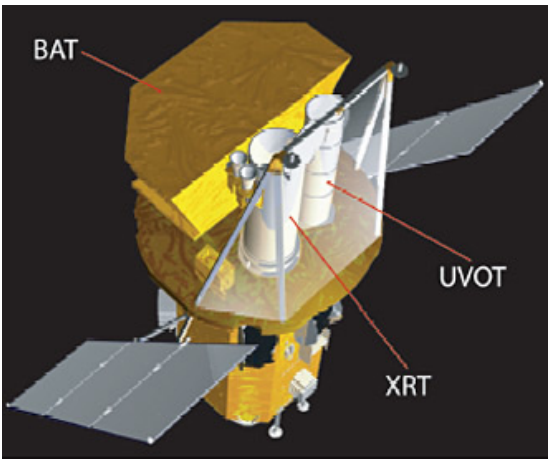

Figure 3.1: Swift Instrumentation and Swift's three scientific instruments: BAT, XRT and UVOT. Figure taken from: NASA/Goddard Space Flight Center.

of 90 minutes, and it weighs 1500 kilogrammes. *Swift* has the main characteristic of a fast response (can turn 50 degrees in 75 seconds or less) and a precise positioning (determines the position to within an error $\sim 3'$ after a few seconds of a burst triggered). *Swift* has worked for 12 years, and triggered more than 1000 bursts.

The unique abilities of the *Swift* satellite, has lead to many discoveries. For instance, it discovered short GRB afterglows (GRBs 050509B, 050709, 050724, etc.) and many of their host galaxies. It has revealed the characteristics of the very early afterglow (canonical X-ray light curve, X-ray flares

and chromatic afterglows), and low-luminosity bursts (e.g. GRB 060218), achieved good multi-band observations of many bursts, and finally detected the extremely high-z record GRB (GRB 090423 [z=8.3] and GRB 090429B [z=9.4]). All this has created a new era in the study of gamma-ray bursts.

Swift has three instruments (see Fig. 3.1) which have different energy bands: Burst Alert Telescope (BAT), X-ray Telescope (XRT) and Ultravilet/optical Telescope (UVOT). BAT [72] energy range is from 15 keV to 150 keV with an energy resolution of 7 keV and an accurate position of $1''$-$4''$. It can achieve rapid position after a GRBs was triggered, and guide the XRT and UVOT and other telescope multi-band follow-up observations. XRT [73] operates in the energy range 0.3-10 keV, the sensitivity can reach 2×10^{-14} erg s^{-1} cm^{-2} after 10^4 seconds. It is used to rapidly detect X-ray radiation and further positioning. UVOT [74] operates in the energy range 170-650 nm, the observations can reach 24 magnitude after 10^3 seconds.

3.2 Magnitudes, colors, and photometric systems

In the observations of GRB afterglow, we usually refer to the use of the photometric systems, here we briefly discuss these. Magnitude is used to measure the luminance of stars. The smaller the value, the brighter it is. It can be expressed from the flux as

$$\mathrm{m} = -2.5\log_{10}\left(\frac{F}{F_0}\right) = -2.5\log_{10}(\mathrm{F}) + \mathrm{ZP}, \tag{3.1}$$

where F_0 is the flux of an object with magnitude equal to zero, and ZP= 2.5 $\log_{10}$ (F_0), which is so-called the zero-point. The measured quantity F depends on the response function of the system and the integration over wavelength. Color is the magnitude difference between any two bands. When we talk about the photometric system, we usually refer to the setting of the system responses and the definition of the zero-point. Two major systems are often used to select zero points: the Vega system and the AB (ABsolute) system. The Vega system is defined such that Vega is 0 magnitude in all used bands. It can be denoted as $\mathrm{mag_{Vega}} = 0$ and $\mathrm{colors_{Vega}} = 0$. The AB magnitude system is defined such that the flux density of magnitude zero-point is 3631 Jy for all considered bands. The corresponding magnitude of a monochromatic flux density, F_ν, is given by

$$\mathrm{m_{AB}} = -2.5\log_{10}\left(\frac{F_\nu}{3631\mathrm{Jy}}\right). \tag{3.2}$$

The common photometric systems are: the Johnson photometric system and Johnson extensions, 2MASS JHKs and SDSS u'g'r'i'z'. The Johnson UBV

photometric system (also called Johnson-Morgan photometric system) [75], is one of the earliest and most used of the standard photometric system. Initially, it contained three bands: U (ultraviolet), B (blue) and V (visual). Later, it has been extended many times, R and I band (Johnson) and the near-IR bands (ZJHKLMQ) were added. The 2MASS JHKs system is similar to the Johnson JHK system, the main difference being that Ks has a different feature. The Sloan Digital Sky Survey (SDSS) system used a five filter (u'g'r'i'z') photometric system.

3.3 Ground-based optical and near-IR observations, and GCN operating principle

GRB afterglow emission are usualy observable up to several hours or even days and longer. The discovery of the afterglow enables us to have enough time to mobilise various telescopes of multi-band observation to get more information. The optical afterglow observation is made by target of opportunity observation by ground-based telescope after they are triggered. At present, there are many ground-based telescopes that perform optical afterglow observations. They are distributed in different countries. The ground-based optical and near-IR telescopes that are used in the thesis, are: *GROND*, *ROTSE-III*, *TAROT*, *RAPTOR*, and *REM*,*VLT*; *TLS*; *TNG*; *SMARTS*. Below we take GROND as an example and introduce its relevant parameters.

In recent years, the observations of the optical afterglow by ground-based telescopes had a very extensive development. One prominent example is the *Gamma-Ray Burst Optical/NIR Detector* (*GROND*) [76; 77]. GROND was commissioned at the MPI/ESO 2.2 m telescope at La Silla (Chile), and it become operational in 2007. GROND is an imaging instrument and its goals include: (i) to identify the GRB afterglow, (ii) to measure the spectral energy distribution, (iii) to determine its photometric redshift. GROND has been designed for rapid observations of GRBs, with the unique capability of a simultaneous seven filter band imaging with Sloan g'r'i'z', four visual channels to near-infrared JHK, three NIR channels. This allows for an immediate photometric redshift determination.

The gamma-ray burst coordinates network (GCN), is a system that reports GRB location information (called notices) when a burst is detected by various instruments. Another important role is that the GCN also automatically receives and distributes messages, called circulars, which provides the follow-up observations to the community. Follow-up observations can then be made by space-based and ground-based observatories.

4. Summary of My Works

4.1 A Correlated Study of Optical and X-ray Afterglows of GRBs

In paper I, I compare the light curves in the X-ray, and in the optical bands for a sample of 87 bursts, in order to test the external shock models.

4.1.1 Context and aim

The standard afterglow model (see §2.4.2) has been successful to explain the data in the pre-*Swift* era. However, the *Swift* satellite [16] has provided an unprecedented sample of long time series of broad energy band observations of bursts. Simultaneous observations with the *Swift* instruments BAT, XRT, UVOT, and ground-based optical telescopes have revolutionized our understanding but have also revealed some critical problems with the standard model [e.g., 78; 79]. For instance, in contrast to the expected results from the standard model, many bursts showed a chromatic behavior between the X-ray and optical bands, that is, showing different behaviors at different frequencies. In recent years, more and more ground-based optical telescopes with increasing sensitivity have accumulated a rich collection of optical afterglows, which allows us to test various external shock models with a large sample.

In this paper, we test the external shock models, using the bursts which have simultaneous X-ray and optical data, considering the break behavior.

4.1.2 Results and conclusions

The main results can be addressed as follows:

(i) A dominant fraction (62%) of the GRBs are consistent with the standard afterglow model (both ISM and Wind models, see §2.4.1, $\alpha_x - \alpha_o \in$ [-0.25,0.25]). When more advanced modeling is invoked (such as energy injection and jet break models, see §2.4.3 and §2.4.4), up to 91% of the bursts in our sample are consistent with the external shock model ($\alpha_x - \alpha_o \in$ [-0.50,0.50]). This is illustrated in Fig. 4.1 which shows the $\alpha_x - \alpha_o$ relation based on different external shock models. Here α_x and α_o are the temporal indices of the X-ray and the optical afterglow light curve, respectively.

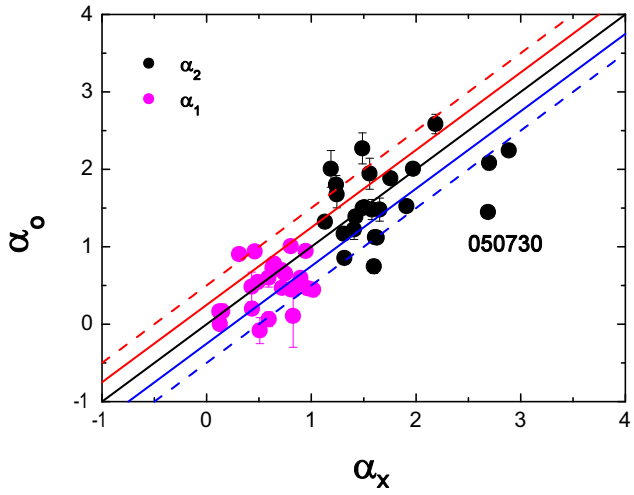

Figure 4.1: The power-law indices for the light-curve decay. The black solid line indicates where are the X-ray and optical temporal indices are equal and the red and blue solid line indicates where $\alpha_{\rm x} = \alpha_{\rm o} \pm 0.25$, which is expected for the standard forward shock model with ISM and wind-like environments. The red and blue dashed lines are $\alpha_{\rm x} = \alpha_{\rm o} \pm 0.5$, which is expected for the energy injection case in a ISM and a wind-like environment, see Paper I.

(ii) Only 9 cases have afterglow light-curves that match the self-similar relativistic blastwave shocks, having a single power law decay in both energy bands, which are observed during their entire duration. An example is GRB 050603 which is shown in Figure 6 in Paper I.

(iii) A large fraction (61%) of bursts are consistent with occurring in a constant interstellar density medium (ISM: $\alpha_x - \alpha_o \in$ [0.0,0.25]) while only 39% of them occur in a wind-like medium (wind: $\alpha_x - \alpha_o \in$ [-0.25,0.0]).

(iv) No cases can be explained by the cooling frequency crossing the X-ray or optical band. Figure 17 in Paper I, shows the distributions of the change in temporal slope ($\Delta\alpha$) between the X-ray with the optical bands. We found that no cases can be explained by the cooling spectral break, since it required $\Delta\alpha$=0.25, and no GRB satisfied this requirement.

(v) An interesting finding is that in nearly half of all cases the plateau phase (energy injection phase) changes directly into the jet decay phase.

We conclude that in general most GRBs are consistent with the external-shock model predictions.

4.2 A Large Catalog of Multi-wavelength GRB Afterglows I: Color Evolution and Its Physical Implication

In paper II, I study the afterglow by analysing the temporal evolution of color indices (CI), defined as the magnitude difference between two filters. They can be used to study the energy spectrum with a good temporal resolution, even when high-resolution spectra are not available.

4.2.1 Context and aim

Ever since the first observation of an optical afterglow (GRB 970228) by BeppoSAX [80] and the launch of the *Swift* satellite more than ten years ago ([16]), many ground-based optical telescopes, with increasing sensitivity, have accumulated a rich collection of optical afterglows. This allows us to study extensively either their multi-band light curves [8; 37; 64; 81–85], or their spectral energy distributions (SEDs) derived from simultaneous multi-band photometry [66; 83–87]. The multiband light curve and CI evolution for GRB 080413B are shown as a typical example in Figure 12 of Paper II. Over most of the observed period the CI does not vary. Large variation however do occur at late times and coincides with a break in the light curves.

Our aim is to study the temporal variability of color indices and explore its physical implications.

In Paper II, I present a statistical analysis of CI based on a large sample of 70 GRBs. I use the CI as a probe to test the standard afterglow models by performing a systematic study to find the temporal evolution of them. We categorize the bursts into two samples based on how well the color indices are evaluated. The Golden sample includes 25 bursts mainly observed by GROND, and the Silver sample includes 45 bursts, observed by other telescopes.

4.2.2 Results

The key results are the following:

(i) I find that 96% of color indices do not vary over time, which means that the spectral slope does not change. Fig. 4.2 shows the evolutions of all CIs with time for all bursts, and most CIs located between -1 to 1. This can be accounted for the simplest external forward shock model.

(ii) The remaining 4% of color indices show significant variation that appear during various limited periods. Several different physical reasons could cause the observed variations: the cooling frequency crosses the studied energy bands, an additional SNe emission emerges during the late optical afterglow, an early dust extinction change and the transition from reverse shock to for-

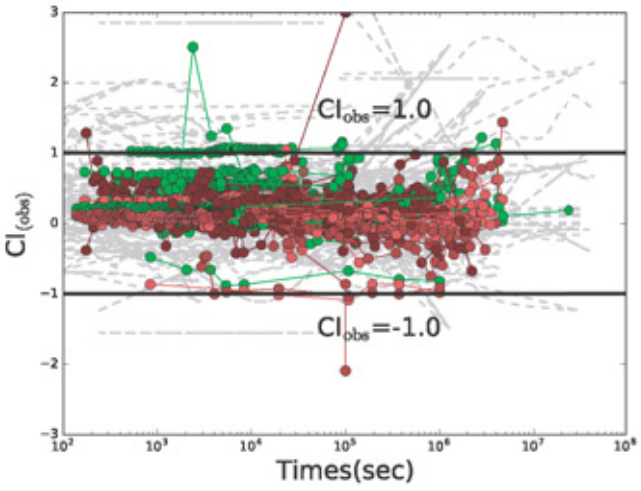

Figure 4.2: In general the CI do not vary with time, as shown by the temporal evolution of all CI for all bursts. The Silver sample is in grey, while each color represents a different combination of bands for the Golden sample. Two horizontal black lines are CI equal -1 and 1, respectively. See Paper II for details.

ward shock emission. Fig. 4.3 shows the ratios of *variable* CI associated to a given phenomenon to the total number of *variable* CI in each time interval.

The temporal evolution of ratios has two peaks among the positive ΔCIs, the first one at $\sim$ 500 seconds and the second one at $\sim 10^6$ seconds. We find that the early peak, corresponding to around 12% of the ΔCIs, are consistent with being dominated by dust extinction. The later peak could be produced by the concurring effect of cooling in a wind-like medium, including 30% of the variable CIs.

Likewise, there are two peaks among the negative ΔCIs, one at $\sim$ 100 seconds, and another one at $\sim 10^5 - 10^6$ seconds. The latter peak is consistent with effect of cooling in a ISM environment, corresponding to $\sim$ 43 % Δ CIs. For the bursts which exhibit a color change at around 100 seconds, the most natural interpretation is the transition from reverse shock to forward shock emissions. This case include $\sim$ 5 % Δ CIs.

Finally, emerging SNe, correspond to 10% of the cases.

(iii) We performed various corrections, such as, subtracted the flux contribution from the host galaxy, converted Vega to AB system, removed the Galactic and host galaxy extinctions, and performed a spectral k-correction. We then studied the distribution of various color indices. The distributions of color indices is shown in Figure 9 of Paper II. We find that most CIs gener-

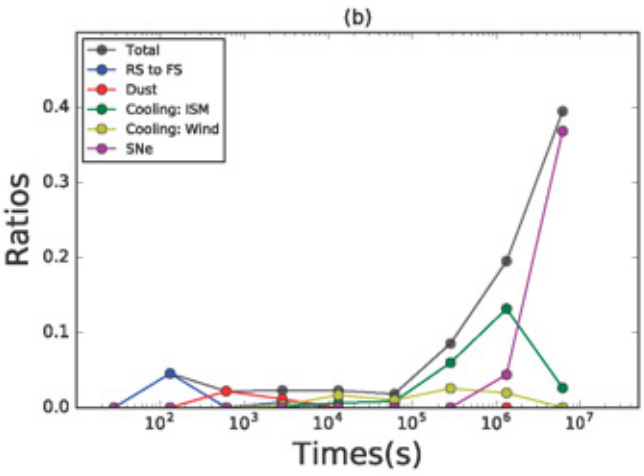

Figure 4.3: The panel presents the ratios of *variable* CI associated to a given phenomenon to the total number of *variable* CI in each time interval (see text for detailed explanations). Different colors represent different phenomena [Paper II].

ally present the same peak value, ~ 0.2. This is consistent with the standard afterglow model with an intrinsic single power-law spectral slope. Two significantly inconsistent peaks are found in the UV bands, which is also consistent with the prediction that the intrinsic reddening is more significant in the high energy bands. We here clarify that there exists an additional reddening.

(iv) After performing all the corrections for the data, we test whether there exists an additional reddening by analyzing the spectral energy distribution (SED). Fig. 4.4 shows the SED of the afterglow from a wide-band observations. The SED of the optical transient, which is derived from the average CI, present a deviated single power-law spectral slope. This implies that the traditional extinction models could be not accurate enough to describe the extinction characteristics for some GRBs.

(v) We then studied the evolution of the mean color indices for different emission episodes. We find that 86% of colors in the 70 bursts show constancy between one component and the following one. The 14% color index that vary occur mainly at the late GRB-SNe bump, the flare and early reversed-shock emission components. The CI correlation between one component and its following one was shown in Figure 14 in Paper II. We find that most CIs are clustered around the equal line, which indicates that the data is consistent with the standard afterglow model with an instincsic power-law spectral slope.

(vi) We further performed a statistical analysis of various observational properties and model parameters (spectral index $\beta_o^{\rm CI}$, electron spectral indices $p^{\rm CI}$, etc) using color indices, and find that they also are consistent with the

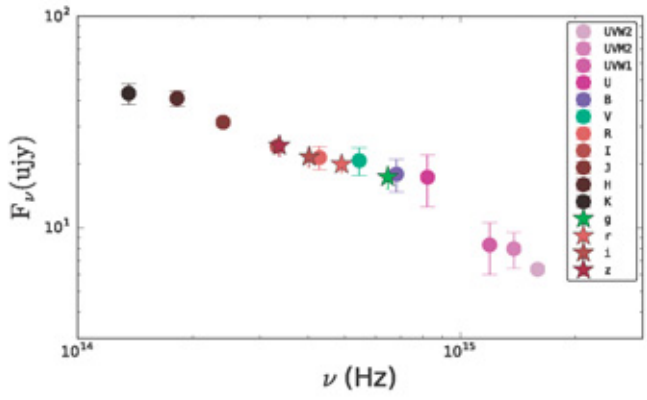

Figure 4.4: The SED of afterglow present a deviated single power-law spectral slope. The star points represent the Golden griz bands while the circular points represent the Silver UBVRI bands [Paper II].

external shock models. The distributions of spectral indices $\beta_o^{\rm CI}$ is shown in Figure 15 in Paper II, and the observed electron spectral indices $p^{\rm CI}$ is shown in Figure 16 in Paper II.

(vii) We further used the closure relations to compute the electron index p from the temporal index α which was obtained by fitting the light curve, or the spectral index β_o (searched from the literature). We then derived the theoretical CIs using the p values and compared them to the observed CIs, see Figure 17 in Paper II. We found they still clustered around the equal line. This also indicates that the data are consistent with the external shock models.

We conclude that most CI are constant, and consistent with the prediction by the expected standard afterglow model. The variable CI indicate that more phenomenon are involved. The evolution of the cooling spectral break and late-SN emission component can account for most of the variable CI.

4.3 Constraining the Type of Central Engine of GRBs with *Swift* data

In paper III, I study the energetics of GRBs that can be inferred from the afterglow observations, in particular bursts which have a plateau phase. Using this information, I analyse the limits it sets on what the central engine can be, if it is a magnetar or a spinning black hole.

4.3.1 Context and motivation

The central engine of gamma-ray bursts is still poorly known, since it cannot be directly observed by electromagnetic emission. However, properties of the central engine can be inferred from current observation. There are two main progenitor models for the central engine of GRB (see §2.1): a fast-rotating black hole and a rapidly spinning magnetar [39].

The progenitor of a short burst is considered to be two neutron stars that merge, while long burst progenitor are from the collapse of a massive star into a black hole. Short GRBs are typically considered to have a magnetars central engine. Both two events eventually create a black hole with a disk of material around it. In paper III, our goal is to find evidence of a black hole central engine.

An X-ray shallow decay phase (or plateau) is commonly observed in *Swift* light curves [7; 88; 89]. An example (GRB 060607A) is given in Figure 1 of Paper III. Such a plateau phase can be interpreted as evidence for long-lasting activity of the central engines, such as an energy injection into the external shock or a refreshed external shock emission [e.g., 7; 34; 36; 49; 50; 56; 88; 90–94]. Such activity can be provided by either a millisecond magnetar with the injected luminosity $L(t) \simeq L_0(t/t_0)^{-q}$ or a fast-rotating black hole.

Since both models are likely involved in such observed characteristics, we extensively searched the *Swift*/XRT light curves with a plateau phase, and that were detected before may 2017. We totally obtained 101 GRBs (with known redshifts) in our sample. We then calculate the afterglow kinetic energy $E_{\rm K,iso}$ and the X-ray energy release $E_{\rm X,iso}$ during the plateau phase for each individual GRB, and characterize them into three categories based on how likely they may harbor a black hole central engine.

4.3.2 Results and conclusions

Our results are the following:

(i) We find that 9 GRBs, which show $E_{\rm X,iso}$ already exceed the energy budget 2×10^{52} erg (see Fig. 4.5) for a magnetar, see §2.1. These GRBs are defined as the Gold sample. In addition, there are 69 GRBs, although $E_{\rm X,iso}$ is less than the budget, $E_{\rm K,iso}$ is greater than the budget. These are defined as the Silver sample. The remaining 23 GRBs have energies that are not over the budget. These are defined as the Bronze sample. The conclusion that can be drawn is that $\sim 80\%$ of the GRBs in our sample are operated by a black hole while the remaining $\sim 20\%$ could harbour a magnetar central engine. We note that this is under the assumption that magnetars emit their energy isotropically.

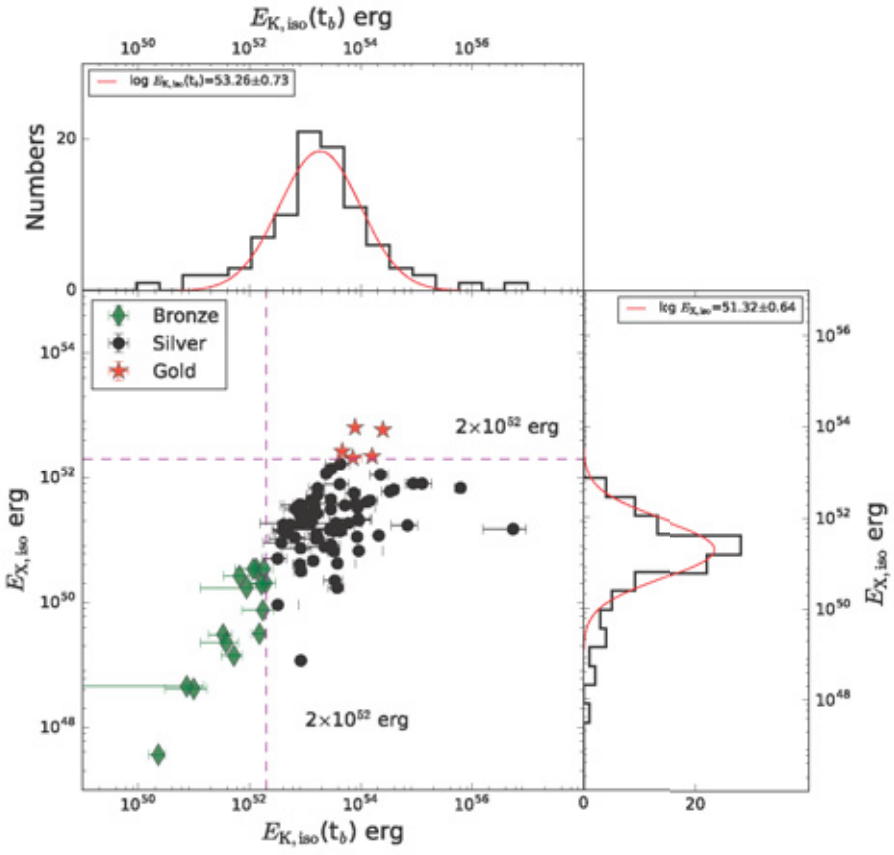

Figure 4.5: The $E_{\rm X,iso}$ compared against the $E_{\rm K,iso}(t_b)$ with their distributions (black solid-lines) and the best Gaussian fits (red solid-lines). Different colors of scatter data points represent different sub-samples (Gold, Silver and Bronze). Two dash-lines represent $E_{\rm X,iso}$ and $E_{\rm K,iso}(t_b)$ equal 2×10^{52} erg, respectively [Paper III].

(ii) By deriving the physical parameters of the putative black hole, we then test the black hole parameters (rotation parameter $a_\bullet$, luminosity injection q, and the correlation of $a_\bullet - q$) with the Blandford & Znajek (BZ) mechanism (see §2.1), and find that the observations of the 'Gold' and 'Silver' samples are consistent with the expectation of the mechanism (see Fig. 4.6).

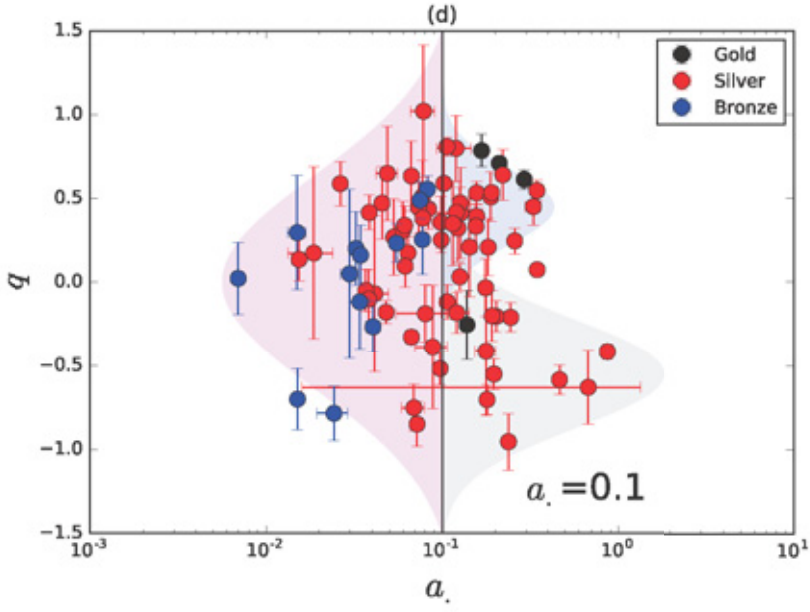

Figure 4.6: The luminosity injection index q compared to the rotation parameter $a_\bullet$. Different colors of the points represent different sub-samples, the black perpendicular line represent $a_\bullet$=0.1, and different color dash-area describe q with different distributions for different $a_\bullet$ values [see further details in Paper III].

Since the Bronze sample bursts could still have a BH central engine, we also calculate $a_\bullet$ for them. Interestingly, we found all Bronze sample bursts have $a_\bullet < 0.1$ (see detail discussion in §3.1 of Paper III).

(iii) We also test the Silver and Bronze samples with the magnetar model, and find that the magnetar surface magnetic filed (B_p) and initial spin period (P_0) fall into a reasonable range for the Bronze sample but not for the Silver sample (see Fig. 4.7). This implies that the Bronze sample is consistent with the magnetar central engine model, but the Silver sample, in general, is inconsistent with the magnetar model.

Our analysis, therefore, supports the conclusion that most GRBs have a black hole central engine.

(iv) We further perform a statistical analysis of various observational prop-

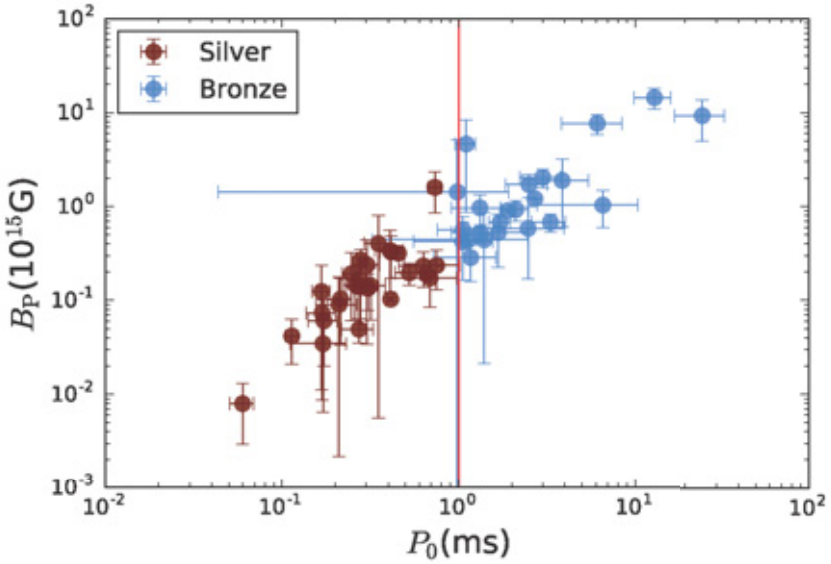

Figure 4.7: The inferred magnetar parameters, initial spin period P_0 versus surface polar cap magnetic field strength B_p, derived for the Bronze samples. The vertical solid line is the breakup spin-period for a neutron star [9] [Paper III].

erties (temporal index α, spectral indices Γ, break time t_b, etc) and model parameters (electron spectral index p, energy injection parameters q, jet opening angle θ_j, radiative efficiency η, etc) for our samples. We find that two candidate samples (Golden+Silver and Bronze), in general, show different statistical characteristics.

(v) 4 out of 5 short GRBs cluster into the Bronze sample. This is consistent with short GRBs coming from neutron star mergers, and have a lower energy compared to black holes.

5. Conclusions and Outlook

The external shock models have been widely used to interpret the broad-band afterglow data of gamma-ray bursts. According to the prediction of the models, the temporal breaks in different energy bands should be achromatic, namely, the break time at different frequencies should be same. However, the multi-wavelength observations in the *Swift* era have revealed a chromatic behavior in broad-band afterglow, which casting doubt on the multi-bands GRB afterglow has an external shock origin.

The central engine of gamma-ray bursts is poorly known. There exist two types of central engine that have been widely discussed in recent years: a fast rotating black hole and rapidly spinning magnetar. An important question is whether the central engine of GRB is more likely to be a black hole or a magnetic star. What is the approximate ratio between them? The maximum energy budget of the initial spin energy is limited to $E_{\rm rot} \sim 2 \times 10^{52}$ erg for magnetars but not for a black hole, this provides a good clue to identifying the type of GRB central engine.

An increasing number of multi-bands observational data provide a good chance to detect various theoretical models. This thesis focuses on to explain the multi-bands observed data with various theoretical models mainly based on the afterglow emission phase. i) In the *Swift* era, accumulated a rich afterglow observation data have been challenging the traditional standard afterglow model. Using the multi-bands observed data to test various external shock models, I conclude that a half fraction GRBs still can be explained by the standard afterglow synchrotron model directly, when more detail external shock models are involved, up to 90%. ii) The evolution of color indices based on a large GRBs sample reveals two classification groups: constant vs. vary. I conclude that different groups may have different physical reasons, I also develop the theory to interpret different types of color indices. iii) I show that most of the bursts the energy exceed the maximum energy budget defined by an initial spin energy of the magnetar $E_{\rm rot} \sim 2 \times 10^{52}$ erg, I conclude that the center engine of GRBs is more likely to be a black hole.

During the course of the work for papers I-III, I initiated two investigations that did not fit into the papers, but address important topics that can related to this thesis.

(i) What is the extinction curve of the host galaxy? One of the most im-

portant issue in astrophysics is that how to accurately describe the host extinction curve. The host extinction of gamma-ray bursts information is still poorly known. A possible method is to assume that the X-ray and the optical afterglow come from the same synchrotron emission. According to standard afterglow model, the spectral index between the X-ray and the optical have two equations: if cooling frequency lie between two bands, $\beta_x=\beta_o+1/2$, otherwise $\beta_x=\beta_o$. Therefore, our motivation is: we assume the X-ray and the optical afterglow abide by standard afterglow model, and using the corrected X-ray SED as the standard to derive the extinction value of the optical bands. We first correct the X-ray afterglow data and derive the SED, then fit the SED with a power-law model (or broken power-law model) and extend to the optical energy regime. If without the extinction, the optical data should be located on the model function line. So this provides us with a method to derive an empirical extinction curve based on our large sample.

(ii) Do the X-ray and optical afterglows come from the same emission source? Another hot question in the gamma-ray bursts field is whether the X-ray and the optical afterglow come from the same emission component. As described by fireball model, the afterglow emission come from the external shock sweet up the interstellar medium outside. According to the standard afterglow model, the X-ray and optical afterglow emission can be described from the same synchrotron emission process. One questions is do they really come from the same synchrotron emission component? Are they from the same site? If they are, why do they show so different light curve features? If they are not, why are their SEDs consistent with the predictions of the afterglow synchrotron model for same cases? Therefore, so one question we can address is that: How many bursts present an achromatic light curve? And how many bursts have a SED that is consistent with the synchrotron predictions? And also how about the time-resolution spectrums? How many bursts abide all?

Sammanfattning

Gamma-ray bursts är de största explosionerna i Universum och härrör från kollapser av olika typer av stjärnor till svarta hål. Efter en energetisk, inledande fas av gamma-strålning, som typiskt pågår under knappt en minut, startas en efterglödsfas. Under denna fas observeras strålning i längre våglängder, t.ex. i röntgen och i visuellt ljus. Denna fas kan pågå i flera veckor och observationer av den kan ge viktig information om explosionens energibudget, utflödets struktur och information om det omgivande mediet (CBM). Standardmodellen innefattar en enda strålningskomponent som skapas av synchrotronstrålning från ett eldkolt som rör sig in i CBM. Flera andra faktorer kan dock påverka det vi observerar. Detta kan vara variationer i CBM, förlängd energitillförsel från de centrala delarna, jetstrålens geometri, och effekter beroende på skillnad mellan siktlinjen jetstrålens riktning. Alla dessa effekter ger an utvidgad standardmodell.

I denna avhandling har jag studerat efterglödsobservationerna ur ett globalt perspektiv genom att analysera stora datagrupper av GRBs för finna generella trender och egenskaper. I paper I jämförde jag ljuskurvor in röntgenstrålning med dem i synligt ljus i en grupp på 87 GRBs. I endast 9 fall passar den enklaste standardmodellen, med en intensitet som avtar som en potenslag med tiden i alla observerade energiband. Om man tar med de andra faktorerna som kan påverkar det vi observerar så finner jag att 91% av GRB i min analysgrupp kan beskrivas av den utvidgade standardmodellen. Ett intressant resultat är att i nästan hälften av alla fall så övergår platåfasen (energitillförselfasen) direkt till jetstrålefasen. I paper II studerade jag efterglöden genom att analysera tidsutvecklingen av färgindexet, vilket definieras som skillnaden i magnitud mellan två olika filter. Färgindexen kan användas för att studera energispektrumets form med god tidsupplösning även i de fall högupplösta spectra inte är mätta. Jag fann att de flesta färgindexen inte varierar med tiden, vilket betyder att formen på spektrumet inte ändras, detta även mellan olika faser i efterglödsljuskurvan. I de fall en variation kunde uppmätas så skedde variationen under begränsade tidsperioder. Vi föreslår att dessa variationer beror på att synchrotronstrålningens kylfrekvens passerar obserationsbanden och i andra fall beror på att den underliggande supernovan blir synlig. I paper III studerade jag explosionens totala energi, vilken kan uppskattas genom att undersöka efterglöden. Med denna information undersöker jag vilken typ av kompakt ob-

jekt som ligger i centrum och driver explosionen, antingen en magnetar eller ett svart hål. Jag fann att omkring 20% av fallen troligen har en magnetar i centrum. För att kontrollera detta resultat så beräknar vi rotationsenergin och rotationsperioden hos svarta-hålfallen och den ursprungliga rotationsperioden och yt-magnetfältet hos magnetarerna. Vi fann att värdena motsvarar de förväntade.

References

[1] **https://gammaray.nsstc.nasa.gov/batse/grb/skymap/**. xvii, 24

[2] CHRYSSA KOUVELIOTOU, CHARLES A MEEGAN, GERALD J FISHMAN, NARAYANA P BHAT, MICHAEL S BRIGGS, THOMAS M KOSHUT, WILLIAM S PACIESAS, AND GEOFFREY N PENDLETON. **Identification of two classes of gamma-ray bursts**. *Astrophysical Journal*, **413**:L101–L104, August 1993. xvii, 23, 24

[3] ASAF PE'ER. **Physics of Gamma-Ray Bursts Prompt Emission**. *Advances in Astronomy*, **2015**:907321, 2015. xvii, 25

[4] D TIERNEY, S MCBREEN, R D PREECE, G FITZPATRICK, S FOLEY, S GUIRIEC, E BISSALDI, M S BRIGGS, J M BURGESS, V CONNAUGHTON, A GOLDSTEIN, J GREINER, D GRUBER, C KOUVELIOTOU, S MCGLYNN, W S PACIESAS, V PELASSA, AND A VON KIENLIN. **Anomalies in low-energy gamma-ray burst spectra with the Fermi Gamma-ray Burst Monitor**. *Astronomy & Astrophysics*, **550**:A102, February 2013. xvii, 26

[5] P MÉSZÁROS. **Gamma-ray bursts**. *Reports on Progress in Physics*, **69**(8):2259–2321, August 2006. xvii, 33

[6] RE'EM SARI, TSVI PIRAN, AND RAMESH NARAYAN. **Spectra and Light Curves of Gamma-Ray Burst Afterglows**. *The Astrophysical Journal*, **497**(1):L17–L20, April 1998. xvii, 37, 38, 39, 40, 41

[7] BING ZHANG, Y Z FAN, JAROSLAW DYKS, SHIHO KOBAYASHI, PETER MÉSZÁROS, DAVID N BURROWS, JOHN A NOUSEK, AND NEIL GEHRELS. **Physical Processes Shaping Gamma-Ray Burst X-Ray Afterglow Light Curves: Theoretical Implications from the Swift X-Ray Telescope Observations**. *The Astrophysical Journal*, **642**(1):354–370, May 2006. xvii, 45, 46, 47, 49, 61

[8] LI, LIANG, LIANG, EN-WEI, TANG, QING-WEN, CHEN, JIE-MIN, XI, SHAO-QIANG, LÜ, HOU-JUN, GAO, HE, ZHANG, BING, ZHANG, JIN, YI, SHUANG-XI, LU, RUI-JING, LÜ, LIAN-ZHONG, AND WEI, JIAN-YAN. **A COMPREHENSIVE STUDY OF GAMMA-RAY BURST OPTICAL EMISSION. I. FLARES AND EARLY SHALLOW-DECAY COMPONENT**. *The Astrophysical Journal*, **758**(1):27–18, September 2012. xvii, 48, 49, 57

[9] J M LATTIMER AND M PRAKASH. **The Physics of Neutron Stars**. *Science*, **304**(5):536–542, April 2004. xviii, 64

[10] RAY W KLEBESADEL, IAN B STRONG, AND ROY A OLSON. **Observations of Gamma-Ray Bursts of Cosmic Origin**. *Astrophysical Journal*, **182**:L85–, June 1973. 23

[11] B P ABBOTT, R ABBOTT, T D ABBOTT, F ACERNESE, K ACKLEY, C ADAMS, T ADAMS, P ADDESSO, R X ADHIKARI, V B ADYA, C AFFELDT, M AFROUGH, B AGARWAL, M AGATHOS, K AGATSUMA, N AGGARWAL, O D AGUIAR, L AIELLO, A AIN, P AJITH, B ALLEN, G ALLEN, A ALLOCCA, P A ALTIN, A AMATO, A ANANYEVA, S B ANDERSON, W G ANDERSON, S V ANGELOVA, S ANTIER, S APPERT, K ARAI, M C ARAYA, J S AREEDA, N ARNAUD, K G ARUN, S ASCENZI, G ASHTON, M AST, S M ASTON, P ASTONE, D V ATALLAH, P AUFMUTH, C AULBERT, K AULTONEAL, C AUSTIN, A AVILA-ALVAREZ, S BABAK, P BACON, M K M

BADER, S BAE, M BAILES, P T BAKER, F BALDACCINI, G BALLARDIN, S W BALLMER, S BANAGIRI, J C BARAYOGA, S E BARCLAY, B C BARISH, D BARKER, K BARKETT, F BARONE, B BARR, L BARSOTTI, M BARSUGLIA, D BARTA, S D BARTHELMY, J BARTLETT, I BARTOS, R BASSIRI, A BASTI, J C BATCH, M BAWAJ, J C BAYLEY, M BAZZAN, B BÉCSY, C BEER, M BEJGER, I BELAHCENE, A S BELL, B K BERGER, G BERGMANN, S BERNUZZI, J J BERO, C P L BERRY, D BERSANETTI, A BERTOLINI, J BETZWIESER, S BHAGWAT, R BHANDARE, I A BILENKO, G BILLINGSLEY, C R BILLMAN, J BIRCH, R BIRNEY, O BIRNHOLTZ, S BISCANS, S BISCOVEANU, A BISHT, M BITOSSI, C BIWER, M A BIZOUARD, J K BLACKBURN, J BLACKMAN, C D BLAIR, D G BLAIR, R M BLAIR, S BLOEMEN, O BOCK, N BODE, M BOER, G BOGAERT, A BOHE, F BONDU, E BONILLA, R BONNAND, B A BOOM, R BORK, V BOSCHI, S BOSE, K BOSSIE, Y BOUFFANAIS, A BOZZI, C BRADASCHIA, P R BRADY, M BRANCHESI, J E BRAU, T BRIANT, A BRILLET, M BRINKMANN, V BRISSON, P BROCKILL, J E BROIDA, A F BROOKS, D A BROWN, D D BROWN, S BRUNETT, C C BUCHANAN, A BUIKEMA, T BULIK, H J BULTEN, A BUONANNO, D BUSKULIC, C BUY, R L BYER, M CABERO, L CADONATI, G CAGNOLI, C CAHILLANE, J CALDERÓN BUSTILLO, T A CALLISTER, E CALLONI, J B CAMP, M CANEPA, P CANIZARES, K C CANNON, H CAO, J CAO, C D CAPANO, E CAPOCASA, F CARBOGNANI, S CARIDE, M F CARNEY, G CARULLO, J CASANUEVA DIAZ, C CASENTINI, S CAUDILL, M CAVAGLIÀ, F CAVALIER, R CAVALIERI, G CELLA, C B CEPEDA, P CERDÁ-DURÁN, G CERRETANI, E CESARINI, S J CHAMBERLIN, M CHAN, S CHAO, P CHARLTON, E CHASE, E CHASSANDE-MOTTIN, D CHATTERJEE, K CHATZIIOANNOU, B D CHEESEBORO, H Y CHEN, X CHEN, Y CHEN, H P CHENG, H CHIA, A CHINCARINI, A CHIUMMO, T CHMIEL, H S CHO, M CHO, J H CHOW, N CHRISTENSEN, Q CHU, A J K CHUA, S CHUA, A K W CHUNG, S CHUNG, G CIANI, R CIOLFI, C E CIRELLI, A CIRONE, F CLARA, J A CLARK, P CLEARWATER, F CLEVA, C COCCHIERI, E COCCIA, P F COHADON, D COHEN, A COLLA, C G COLLETTE, L R COMINSKY, M CONSTANCIO, L CONTI, S J COOPER, P CORBAN, T R CORBITT, I CORDERO-CARRIÓN, K R CORLEY, N CORNISH, A CORSI, S CORTESE, C A COSTA, M W COUGHLIN, S B COUGHLIN, J P COULON, S T COUNTRYMAN, P COUVARES, P B COVAS, E E COWAN, D M COWARD, M J COWART, D C COYNE, R COYNE, J D E CREIGHTON, T D CREIGHTON, J CRIPE, S G CROWDER, T J CULLEN, A CUMMING, L CUNNINGHAM, E CUOCO, T DAL CANTON, G DÁLYA, S L DANILISHIN, S D'ANTONIO, K DANZMANN, A DASGUPTA, C F DA SILVA COSTA, V DATTILO, I DAVE, M DAVIER, D DAVIS, E J DAW, B DAY, S DE, D DEBRA, J DEGALLAIX, M DE LAURENTIS, S DELÉGLISE, W DEL POZZO, N DEMOS, T DENKER, T DENT, R DE PIETRI, V DERGACHEV, R DE ROSA, R T DEROSA, C DE ROSSI, R DESALVO, O DE VARONA, J DEVENSON, S DHURANDHAR, M C DÍAZ, T DIETRICH, L DI FIORE, M DI GIOVANNI, T DI GIROLAMO, A DI LIETO, S DI PACE, I DI PALMA, F DI RENZO, Z DOCTOR, V DOLIQUE, F DONOVAN, K L DOOLEY, S DORAVARI, I DORRINGTON, R DOUGLAS, M DOVALE ÁLVAREZ, T P DOWNES, M DRAGO, C DREISSIGACKER, J C DRIGGERS, Z DU, M DUCROT, R DUDI, P DUPEJ, S E DWYER, T B EDO, M C EDWARDS, AND EF... **GW170817: Observation of Gravitational Waves from a Binary Neutron Star Inspiral**. *Physical Review Letters*, **119**(1):161101, October 2017. 23

[12] D BAND, J MATTESON, L FORD, B SCHAEFER, D PALMER, B TEEGARDEN, T CLINE, M BRIGGS, W PACIESAS, G PENDLETON, G FISHMAN, C KOUVELIOTOU, C MEEGAN, R WILSON, AND P LESTRADE. **BATSE observations of gamma-ray burst spectra. I - Spectral diversity**. *Astrophysical Journal*, **413**:281–292, August 1993. 25

[13] R D PREECE, M S BRIGGS, R S MALLOZZI, G N PENDLETON, W S PACIESAS, AND D L BAND. **The BATSE Gamma-Ray Burst Spectral Catalog. I. High Time Resolution Spectroscopy of Bright Bursts Using High Energy Resolution Data**. *The Astrophysical Journal Supplement Series*, **126**(1):19–36, January 2000. 25

[14] P MÉSZÁROS AND M J REES. **Optical and Long-Wavelength Afterglow from Gamma-Ray Bursts**. *The Astrophysical Journal*, **476**(1):232–237, February 1997. 25, 39, 40

[15] T J GALAMA, P M VREESWIJK, J VAN PARADIJS, C KOUVELIOTOU, T AUGUSTEIJN, H BÖHNHARDT, J P BREWER, V DOUBLIER, J F GONZALEZ, B LEIBUNDGUT, C LIDMAN, O R HAINAUT, F PATAT, J HEISE, J IN'T ZAND, K HURLEY, P J GROOT, R G STROM, P A MAZZALI, K IWAMOTO, K NOMOTO, H UMEDA, T NAKAMURA, T R YOUNG, T SUZUKI, T SHIGEYAMA, T KOSHUT, M KIPPEN, C ROBINSON, P DE WILDT, R A M J WIJERS, N TANVIR, J GREINER,

E PIAN, E PALAZZI, F FRONTERA, N MASETTI, L NICASTRO, M FEROCI, E COSTA, L PIRO, B A PETERSON, C TINNEY, B BOYLE, R CANNON, R STATHAKIS, E SADLER, M C BEGAM, AND P IANNA. **An unusual supernova in the error box of the γ-ray burst of 25 April 1998**. *Nature*, **395**(6):670–672, October 1998. 26

[16] N GEHRELS, G CHINCARINI, P GIOMMI, K O MASON, J A NOUSEK, A A WELLS, N E WHITE, S D BARTHELMY, D N BURROWS, L R COMINSKY, K C HURLEY, F E MARSHALL, P MÉSZÁROS, P W A ROMING, L ANGELINI, L M BARBIER, T BELLONI, S CAMPANA, P A CARAVEO, M M CHESTER, O CITTERIO, T L CLINE, M S CROPPER, J R CUMMINGS, A J DEAN, E D FEIGELSON, E E FENIMORE, D A FRAIL, A S FRUCHTER, G P GARMIRE, K GENDREAU, G GHISELLINI, J GREINER, J E HILL, S D HUNSBERGER, H A KRIMM, S R KULKARNI, P KUMAR, F LEBRUN, N M LLOYD-RONNING, C B MARKWARDT, B J MATTSON, R F MUSHOTZKY, J P NORRIS, J OSBORNE, B PACZYNSKI, D M PALMER, H S PARK, A M PARSONS, J PAUL, M J REES, C S REYNOLDS, J E RHOADS, T P SASSEEN, B E SCHAEFER, A T SHORT, A P SMALE, I A SMITH, L STELLA, G TAGLIAFERRI, T TAKAHASHI, M TASHIRO, L K TOWNSLEY, J TUELLER, M J L TURNER, M VIETRI, W VOGES, M J WARD, R WILLINGALE, F M ZERBI, AND W W ZHANG. **The Swift Gamma-Ray Burst Mission**. *The Astrophysical Journal*, **611**(2):1005–1020, August 2004. 26, 51, 55, 57

[17] CHARLES MEEGAN, GISELHER LICHTI, P N BHAT, ELISABETTA BISSALDI, MICHAEL S BRIGGS, VALERIE CONNAUGHTON, ROLAND DIEHL, GERALD FISHMAN, JOCHEN GREINER, ANDREW S HOOVER, ALEXANDER J VAN DER HORST, ANDREAS VON KIENLIN, R MARC KIPPEN, CHRYSSA KOUVELIOTOU, SHEILA MCBREEN, W S PACIESAS, ROBERT PREECE, HELMUT STEINLE, MARK S WALLACE, ROBERT B WILSON, AND COLLEEN WILSON-HODGE. **The Fermi Gamma-ray Burst Monitor**. *The Astrophysical Journal*, **702**(1):791–804, September 2009. 26

[18] W B ATWOOD, A A ABDO, M ACKERMANN, W ALTHOUSE, B ANDERSON, M AXELSSON, L BALDINI, J BALLET, D L BAND, G BARBIELLINI, J BARTELT, D BASTIERI, B M BAUGHMAN, K BECHTOL, D BÉDÉRÈDE, F BELLARDI, R BELLAZZINI, B BERENJI, G F BIGNAMI, D BISELLO, E BISSALDI, R D BLANDFORD, E D BLOOM, J R BOGART, E BONAMENTE, J BONNELL, A W BORGLAND, A BOUVIER, J BREGEON, A BREZ, M BRIGIDA, P BRUEL, T H BURNETT, G BUSETTO, G A CALIANDRO, R A CAMERON, P A CARAVEO, S CARIUS, P CARLSON, J M CASANDJIAN, E CAVAZZUTI, M CECCANTI, C CECCHI, E CHARLES, A CHEKHTMAN, C C CHEUNG, J CHIANG, R CHIPAUX, A N CILLIS, S CIPRINI, R CLAUS, J COHEN-TANUGI, S CONDAMOOR, J CONRAD, R CORBET, L CORUCCI, L COSTAMANTE, S CUTINI, D S DAVIS, D DECOTIGNY, M DEKLOTZ, C D DERMER, A DE ANGELIS, S W DIGEL, E DO COUTO E SILVA, P S DRELL, R DUBOIS, D DUMORA, Y EDMONDS, D FABIANI, C FARNIER, C FAVUZZI, D L FLATH, P FLEURY, W B FOCKE, S FUNK, P FUSCO, F GARGANO, D GASPARRINI, N GEHRELS, F X GENTIT, S GERMANI, B GIEBELS, N GIGLIETTO, P GIOMMI, F GIORDANO, T GLANZMAN, G GODFREY, I A GRENIER, M H GRONDIN, J E GROVE, L GUILLEMOT, S GUIRIEC, G HALLER, A K HARDING, P A HART, E HAYS, S E HEALEY, M HIRAYAMA, L HJALMARSDOTTER, R HORN, R E HUGHES, G JÓHANNESSON, G JOHANSSON, A S JOHNSON, R P JOHNSON, T J JOHNSON, W N JOHNSON, T KAMAE, H KATAGIRI, J KATAOKA, A KAVELAARS, N KAWAI, H KELLY, M KERR, W KLAMRA, J KNÖDLSEDER, M L KOCIAN, N KOMIN, F KUEHN, M KUSS, D LANDRIU, L LATRONICO, B LEE, S H LEE, M LEMOINE-GOUMARD, A M LIONETTO, F LONGO, F LOPARCO, B LOTT, M N LOVELLETTE, P LUBRANO, G M MADEJSKI, A MAKEEV, B MARANGELLI, M M MASSAI, M N MAZZIOTTA, J E MCENERY, N MENON, C MEURER, P F MICHELSON, M MINUTI, N MIRIZZI, W MITTHUMSIRI, T MIZUNO, A A MOISEEV, C MONTE, M E MONZANI, E MORETTI, A MORSELLI, I V MOSKALENKO, S MURGIA, T NAKAMORI, S NISHINO, P L NOLAN, J P NORRIS, E NUSS, M OHNO, T OHSUGI, N OMODEI, E ORLANDO, J F ORMES, A PACCAGNELLA, D PANEQUE, J H PANETTA, D PARENT, M PEARCE, M PEPE, A PERAZZO, M PESCE-ROLLINS, P PICOZZA, L PIERI, M PINCHERA, F PIRON, T A PORTER, L POUPARD, S RAINÒ, R RANDO, E RAPPOSELLI, M RAZZANO, A REIMER, O REIMER, T REPOSEUR, L C REYES, S RITZ, L S ROCHESTER, A Y RODRIGUEZ, R W ROMANI, M ROTH, J J RUSSELL, F RYDE, S SABATINI, H F W SADROZINSKI, D SANCHEZ, A SANDER, L SAPOZHNIKOV, P M SAZ PARKINSON, J D SCARGLE, T L SCHALK, G SCOLIERI, C SGRÒ, G H SHARE, M SHAW, T SHIMOKAWABE, C SHRADER, A SIERPOWSKA-BARTOSIK, E J SISKIND, D A SMITH, P D SMITH, G SPANDRE, P SPINELLI, J L STARCK, T E STEPHENS, M S STRICKMAN, A W STRONG, D J SUSON, H TAJIMA, H TAKAHASHI, T TAKAHASHI, T TANAKA, A TENZE,

S Tether, J B Thayer, J G Thayer, D J Thompson, L Tibaldo, O Tibolla, D F Torres, G Tosti, A Tramacere, M Turri, T L Usher, N Vilchez, V Vitale, P Wang, K Watters, B L Winer, K S Wood, T Ylinen, and M Ziegler. **The Large Area Telescope on the Fermi Gamma-Ray Space Telescope Mission**. *The Astrophysical Journal*, **697**(2):1071–1102, June 2009. 26

[19] F Ryde, M Axelsson, B B Zhang, S McGlynn, A Pe'er, C Lundman, S Larsson, M Battelino, B Zhang, E Bissaldi, J Bregeon, M S Briggs, J Chiang, F de Palma, S Guiriec, J Larsson, F Longo, S McBreen, N Omodei, V Petrosian, R Preece, and A J van der Horst. **Identification and Properties of the Photospheric Emission in GRB090902B**. *The Astrophysical Journal Letters*, **709**(2):L172–L177, February 2010. 27

[20] M Ackermann, K Asano, W B Atwood, M Axelsson, L Baldini, J Ballet, G Barbiellini, M G Baring, D Bastieri, K Bechtol, R Bellazzini, B Berenji, P N Bhat, E Bissaldi, R D Blandford, E D Bloom, E Bonamente, A W Borgland, A Bouvier, J Bregeon, A Brez, M S Briggs, M Brigida, P Bruel, S Buson, G A Caliandro, R A Cameron, P A Caraveo, S Carrigan, J M Casandjian, C Cecchi, Ö Çelik, E Charles, J Chiang, S Ciprini, R Claus, J Cohen-Tanugi, V Connaughton, J Conrad, C D Dermer, F de Palma, B L Dingus, E do Couto e Silva, P S Drell, R Dubois, D Dumora, C Farnier, C Favuzzi, S J Fegan, J Finke, W B Focke, M Frailis, Y Fukazawa, P Fusco, F Gargano, D Gasparrini, N Gehrels, S Germani, N Giglietto, F Giordano, T Glanzman, G Godfrey, J Granot, I A Grenier, M H Grondin, J E Grove, S Guiriec, D Hadasch, A K Harding, E Hays, D Horan, R E Hughes, G Johannesson, W N Johnson, T Kamae, H Katagiri, J Kataoka, N Kawai, R M Kippen, J Knodlseder, D Kocevski, C Kouveliotou, M Kuss, J Lande, L Latronico, M Lemoine-Goumard, M Llena Garde, F Longo, F Loparco, B Lott, M N Lovellette, P Lubrano, A Makeev, M N Mazziotta, J E McEnery, S McGlynn, C Meegan, P Mészáros, P F Michelson, W Mitthumsiri, T Mizuno, A A Moiseev, C Monte, M E Monzani, E Moretti, A Morselli, I V Moskalenko, S Murgia, H Nakajima, T Nakamori, P L Nolan, J P Norris, E Nuss, M Ohno, T Ohsugi, N Omodei, E Orlando, J F Ormes, M Ozaki, W S Paciesas, D Paneque, J H Panetta, D Parent, V Pelassa, M Pepe, M Pesce-Rollins, F Piron, R Preece, S Raino, R Rando, M Razzano, S Razzaque, A Reimer, S Ritz, A Y Rodriguez, M Roth, F Ryde, H F W Sadrozinski, A Sander, J D Scargle, T L Schalk, C Sgro, E J Siskind, P D Smith, G Spandre, P Spinelli, M Stamatikos, F W Stecker, M S Strickman, D J Suson, H Tajima, H Takahashi, T Takahashi, T Tanaka, J B Thayer, J G Thayer, D J Thompson, L Tibaldo, K Toma, D F Torres, G Tosti, A Tramacere, Y Uchiyama, T Uehara, T L Usher, A J Van der Horst, V Vasileiou, N Vilchez, V Vitale, A von Kienlin, A P Waite, P Wang, C Wilson-Hodge, B L Winer, X F Wu, R Yamazaki, Z Yang, T Ylinen, and M Ziegler. **Fermi Observations of GRB 090510: A Short-Hard Gamma-ray Burst with an Additional, Hard Power-law Component from 10 keV TO GeV Energies**. *The Astrophysical Journal*, **716**(2):1178–1190, June 2010. 27

[21] G Ghirlanda, G Ghisellini, and L Nava. **The onset of the GeV afterglow of GRB 090510**. *arXiv.org*, page L7, August 2009. 27

[22] G Cavallo and M J Rees. **A qualitative study of cosmic fireballs and gamma-ray bursts**. *Monthly Notices of the Royal Astronomical Society*, **183**:359–365, May 1978. 27

[23] Wei-Hua Lei, Bing Zhang, Xue-Feng Wu, and En-Wei Liang. **Hyperaccreting Black Hole as Gamma-Ray Burst Central Engine. II. Temporal evolution of central engine parameters during Prompt and Afterglow Phases**. *arXiv.org*, page arXiv:1708.05043, August 2017. 29

[24] Fan, Y Z and Xu, D. **The X-ray afterglow flat segment in short GRB 051221A: Energy injection from a millisecond magnetar?** *Monthly Notices of the Royal Astronomical Society: Letters*, **372**(1):L19–L22, October 2006. 30

[25] B D Metzger, D Giannios, T A Thompson, N Bucciantini, and E Quataert. **The protomagnetar model for gamma-ray bursts**. *Monthly Notices of the Royal Astronomical Society*, **413**(3):2031–2056, May 2011.

[26] S DALL'OSSO, G STRATTA, D GUETTA, S COVINO, G DE CESARE, AND L STELLA. **Gamma-ray bursts afterglows with energy injection from a spinning down neutron star**. *Astronomy & Astrophysics*, **526**:A121, 2011.

[27] N BUCCIANTINI, B D METZGER, T A THOMPSON, AND E QUATAERT. **Short gamma-ray bursts with extended emission from magnetar birth: jet formation and collimation**. *Monthly Notices of the Royal Astronomical Society*, **419**(2):1537–1545, January 2012.

[28] M G BERNARDINI, S CAMPANA, G GHISELLINI, P D'AVANZO, D BURLON, S COVINO, G GHIRLANDA, A MELANDRI, R SALVATERRA, S D VERGANI, V D'ELIA, D FUGAZZA, B SBARUFATTI, AND G TAGLIAFERRI. **HOW TO SWITCH A GAMMA-RAY BURST ON AND OFF THROUGH A MAGNETAR**. *The Astrophysical Journal*, **775**(1):67, 2013.

[29] B P GOMPERTZ, P T O'BRIEN, G A WYNN, AND A ROWLINSON. **Can magnetar spin-down power extended emission in some short GRBs?** *Monthly Notices of the Royal Astronomical Society*, **431**(2):1745–1751, May 2013.

[30] B P GOMPERTZ, P T O'BRIEN, AND G A WYNN. **Magnetar powered GRBs: explaining the extended emission and X-ray plateau of short GRB light curves**. *Monthly Notices of the Royal Astronomical Society*, **438**(1):240–250, February 2014.

[31] HOU-JUN LÜ AND BING ZHANG. **A TEST OF THE MILLISECOND MAGNETAR CENTRAL ENGINE MODEL OF GAMMA-RAY BURSTS WITH SWIFTDATA**. *The Astrophysical Journal*, **785**(1):74–15, March 2014.

[32] HOU-JUN LÜ, BING ZHANG, WEI-HUA LEI, YE LI, AND PAUL D LASKY. **THE MILLISECOND MAGNETAR CENTRAL ENGINE IN SHORT GRBs**. *The Astrophysical Journal*, **805**(2):89, June 2015. 30

[33] HOU-JUN LÜ AND BING ZHANG. **A TEST OF THE MILLISECOND MAGNETAR CENTRAL ENGINE MODEL OF GAMMA-RAY BURSTS WITH SWIFT DATA**. *The Astrophysical Journal*, **785**(1):74, April 2014. 30

[34] BING ZHANG AND PETER MÉSZÁROS. **Gamma-Ray Burst Afterglow with Continuous Energy Injection: Signature of a Highly Magnetized Millisecond Pulsar**. *The Astrophysical Journal*, **552**(1):L35–L38, May 2001. 30, 41, 42, 61

[35] GEORGE B RYBICKI AND ALAN P LIGHTMAN. **Radiative processes in astrophysics**. *New York*, 1979. 34

[36] A PANAITESCU, P MÉSZÁROS, AND M J REES. **Multiwavelength Afterglows in Gamma-Ray Bursts: Refreshed Shock and Jet Effects**. *The Astrophysical Journal*, **503**(1):314–324, August 1998. 39, 40, 61

[37] A PANAITESCU AND P KUMAR. **Properties of Relativistic Jets in Gamma-Ray Burst Afterglows**. *The Astrophysical Journal*, **571**(2):779–789, June 2002. 57

[38] BING ZHANG AND PETER MÉSZÁROS. **Gamma-Ray Bursts: progress, problems & prospects**. *International Journal of Modern Physics A*, **19**(1):2385–2472, 2004. 40

[39] PAWAN KUMAR AND BING ZHANG. **The physics of gamma-ray bursts & relativistic jets**. *Physics Reports*, **561**:1–109, February 2015. 39, 61

[40] R D BLANDFORD AND C F MCKEE. **Radiation from relativistic blast waves in quasars and active galactic nuclei**. *Monthly Notices of the Royal Astronomical Society*, **180**:343–371, August 1977. 39

[41] BOHDAN PACZYNSKI AND JAMES E RHOADS. **Radio Transients from Gamma-Ray Bursters**. *Astrophysical Journal Letters v.418*, **418**:L5–, November 1993. 39

[42] P MESZAROS AND M J REES. **Gamma-Ray Bursts: Multiwaveband Spectral Predictions for Blast Wave Models**. *Astrophysical Journal Letters v.418*, **418**:L59–, December 1993. 39

[43] Y F HUANG, L J GOU, Z G DAI, AND T LU. **Overall Evolution of Jetted Gamma-Ray Burst Ejecta**. *The Astrophysical Journal*, **543**(1):90–96, November 2000. 40, 41, 43

[44] A PANAITESCU AND P KUMAR. **Analytic Light Curves of Gamma-Ray Burst Afterglows: Homogeneous versus Wind External Media**. *The Astrophysical Journal*, **543**(1):66–76, November 2000. 41

[45] X F WU, Z G DAI, Y F HUANG, AND T LU. **Optical flashes and very early afterglows in wind environments**. *Monthly Notice of the Royal Astronomical Society*, **342**(4):1131–1138, July 2003.

[46] KOBAYASHI, SHIHO AND ZHANG, BING. **Early Optical Afterglows from Wind-Type Gamma-Ray Bursts**. *The Astrophysical Journal*, **597**(1):455–458, November 2003.

[47] SHIHO KOBAYASHI, PETER MSZROS, AND BING ZHANG. **A Characteristic Dense Environment or Wind Signature in Prompt Gamma-Ray Burst Afterglows**. *The Astrophysical Journal*, **601**(1):L13–L16, 2004. 41

[48] P MESZAROS, M J REES, AND R A M J WIJERS. **Viewing Angle and Environment Effects in Gamma-Ray Bursts: Sources of Afterglow Diversity**. *The Astrophysical Journal*, **499**(1):301–308, 1998. 41

[49] Z G DAI AND T LU. **Gamma-ray burst afterglows and evolution of postburst fireballs with energy injection from strongly magnetic millisecond pulsars**. *Astronomy and Astrophysics*, **333**:L87–L90, May 1998. 42, 61

[50] M J REES AND P MÉSZÁROS. **Refreshed Shocks and Afterglow Longevity in Gamma-Ray Bursts**. *The Astrophysical Journal*, **496**(1):L1–L4, March 1998. 42, 61

[51] J E RHOADS. **Gamma-ray burst beaming constraints from afterglow light curves**. *Astronomy and Astrophysics Supplement*, **138**:539–540, September 1999. 43, 44

[52] RE'EM SARI, TSVI PIRAN, AND J P HALPERN. **Jets in Gamma-Ray Bursts**. *The Astrophysical Journal*, **519**(1):L17–L20, 1999. 43, 44

[53] ROGER A CHEVALIER AND ZHI-YUN LI. **Gamma-Ray Burst Environments and Progenitors**. *The Astrophysical Journal*, **520**(1):L29–L32, July 1999.

[54] ROGER A CHEVALIER AND ZHI-YUN LI. **Wind Interaction Models for Gamma-Ray Burst Afterglows: The Case for Two Types of Progenitors**. *The Astrophysical Journal*, **536**(1):195–212, June 2000. 41

[55] A MELANDRI, C G MUNDELL, S KOBAYASHI, C GUIDORZI, A GOMBOC, I A STEELE, R J SMITH, D BERSIER, C J MOTTRAM, D CARTER, M F BODE, P T O'BRIEN, N R TANVIR, E ROL, AND R CHAPMAN. **The Early-Time Optical Properties of Gamma-Ray Burst Afterglows**. *The Astrophysical Journal*, **686**(2):1209–1230, October 2008. 41

[56] RE'EM SARI AND PETER MÉSZÁROS. **Impulsive and Varying Injection in Gamma-Ray Burst Afterglows**. *The Astrophysical Journal*, **535**(1):L33–L37, May 2000. 42, 61

[57] HENDRIK VAN EERTEN AND ANDREW MACFADYEN. **Gamma-Ray Burst Afterglow Light Curves from a Lorentz-boosted Simulation Frame and the Shape of the Jet Break**. *The Astrophysical Journal*, **767**(2):141, April 2013. 43

[58] PAUL C DUFFELL AND ANDREW I MACFADYEN. **Shock Corrugation by Rayleigh-Taylor Instability in Gamma-Ray Burst Afterglow Jets**. *The Astrophysical Journal Letters*, **791**(1):L1, August 2014. 43

[59] D A Frail, S R Kulkarni, R Sari, S G Djorgovski, J S Bloom, T J Galama, D E Reichart, E Berger, F A Harrison, P A Price, S A Yost, A Diercks, R W Goodrich, and F Chaffee. **Beaming in Gamma-Ray Bursts: Evidence for a Standard Energy Reservoir**. *The Astrophysical Journal*, **562**(1):L55–L58, 2001. 45

[60] He Gao, Wei-Hua Lei, Yuan-Chuan Zou, Xue-Feng Wu, and Bing Zhang. **A complete reference of the analytical synchrotron external shock models of gamma-ray bursts**. *New Astronomy Reviews*, **57**(6):141–190, December 2013. 45

[61] Bin-Bin Zhang, En-Wei Liang, and Bing Zhang. **A Comprehensive Analysis of Swift XRT Data. I. Apparent Spectral Evolution of Gamma-Ray Burst X-Ray Tails**. *The Astrophysical Journal*, **666**(2):1002–1011, September 2007. 46

[62] E Troja, G Cusumano, P T O'Brien, B Zhang, B Sbarufatti, V Mangano, R Willingale, G Chincarini, J P Osborne, F E Marshall, D N Burrows, S Campana, N Gehrels, C Guidorzi, H A Krimm, V La Parola, E W Liang, T Mineo, A Moretti, K L Page, P Romano, G Tagliaferri, B B Zhang, M J Page, and P Schady. **Swift Observations of GRB 070110: An Extraordinary X-Ray Afterglow Powered by the Central Engine**. *The Astrophysical Journal*, **665**(1):599–607, August 2007. 47

[63] Liang Li, Xue-Feng Wu, Yong-Feng Huang, Xiang-Gao Wang, Qing-Wen Tang, Yun-Feng Liang, Bin-Bin Zhang, Yu Wang, Jin-Jun Geng, En-Wei Liang, Jian-Yan Wei, Bing Zhang, Ryde, and Felix. **A CORRELATED STUDY OF OPTICAL AND X-RAY AFTERGLOWS OF GRBs**. *The Astrophysical Journal*, **805**(1):13, 2015. 48

[64] En-Wei Liang, Liang Li, He Gao, Bing Zhang, Yun-Feng Liang, Xue-Feng Wu, Shuang-Xi Yi, Zi-Gao Dai, Qing-Wen Tang, Jie-Min Chen, Hou-Jun Lü, Jin Zhang, Rui-Jing Lu, Lian-Zhong Lü, and Jian-Yan Wei. **A COMPREHENSIVE STUDY OF GAMMA-RAY BURST OPTICAL EMISSION. II. AFTERGLOW ONSET AND LATE REBRIGHTENING COMPONENTS**. *The Astrophysical Journal*, **774**(1):13, 2013. 57

[65] M Nardini, G Ghisellini, G Ghirlanda, F Tavecchio, C Firmani, and D Lazzati. **Clustering of the optical-afterglow luminosities of long gamma-ray bursts**. *Astronomy & Astrophysics*, **451**(3):821–833, 2006.

[66] Kann, D A, Klose, S, and Zeh, A. **Signatures of Extragalactic Dust in Pre-Swift GRB Afterglows**. *The Astrophysical Journal*, **641**(2):993–1009, April 2006. 57

[67] D A Kann, S Klose, B Zhang, D Malesani, E Nakar, A Pozanenko, A C Wilson, N R Butler, P Jakobsson, S Schulze, M Andreev, L A Antonelli, I F Bikmaev, V Biryukov, M Böttcher, R A Burenin, J M Castro Cerón, A J Castro-Tirado, G Chincarini, B E Cobb, S Covino, P D'Avanzo, V D'Elia, M Della Valle, A de Ugarte Postigo, Yu Efimov, P Ferrero, D Fugazza, J P U Fynbo, M Gålfalk, F Grundahl, J Gorosabel, S Gupta, S Guziy, B Hafizov, J Hjorth, K Holhjem, M Ibrahimov, M Im, G L Israel, B L Jensen, R Karimov, I M Khamitov, E Klunko, P Kubánek, A S Kutyrev, P Laursen, A J Levan, F Mannucci, C M Martin, A Mescheryakov, N Mirabal, J P Norris, J E Ovaldsen, D Paraficz, E Pavlenko, S Piranomonte, A Rossi, V Rumyantsev, R Salinas, A Sergeev, D Sharapov, J Sollerman, B Stecklum, L Stella, G Tagliaferri, N R Tanvir, J Telting, V Testa, A C Updike, A Volnova, D Watson, K Wiersema, and D Xu. **The Afterglows of Swift-era Gamma-Ray Bursts. I. Comparing pre-Swift and Swift era Long/Soft (Type II) GRB Optical Afterglows**. *arXiv.org*, December 2007.

[68] D A Kann, S Klose, B Zhang, S Covino, N R Butler, D Malesani, E Nakar, A C Wilson, L A Antonelli, G Chincarini, B E Cobb, P D'Avanzo, V D'Elia, M Della Valle, P Ferrero, D Fugazza, J Gorosabel, G L Israel, F Mannucci, S Piranomonte, S Schulze, L Stella, G Tagliaferri, and K Wiersema. **The Afterglows of Swift-era Gamma-Ray Bursts II.: Type I GRB versus Type II GRB Optical Afterglows**. *arXiv.org*, April 2008.

[69] A PANAITESCU AND W T VESTRAND. **Taxonomy of gamma-ray burst optical light curves: identification of a salient class of early afterglows**. *Monthly Notices of the Royal Astronomical Society*, **387**(2):497–504, 2008.

[70] A PANAITESCU AND W T VESTRAND. **Optical afterglows of gamma-ray bursts: peaks, plateaus and possibilities**. *Monthly Notices of the Royal Astronomical Society*, **414**(4):3537–3546, 2011. 48

[71] LIANG, EN-WEI, ZHANG, BIN-BIN, AND ZHANG, BING. **A Comprehensive Analysis of Swift XRT Data. II. Diverse Physical Origins of the Shallow Decay Segment**. *The Astrophysical Journal*, **670**(1):565–583, November 2007. 49

[72] SCOTT D BARTHELMY, LOUIS M BARBIER, JAY R CUMMINGS, ED E FENIMORE, NEIL GEHRELS, DEREK HULLINGER, HANS A KRIMM, CRAIG B MARKWARDT, DAVID M PALMER, ANN PARSONS, GORO SATO, MASAYA SUZUKI, TADAYUKI TAKAHASHI, MAKOTA TASHIRO, AND JACK TUELLER. **The Burst Alert Telescope (BAT) on the SWIFT Midex Mission**. *Space Science Reviews*, **120**(3-4):143–164, 2005. 52

[73] DAVID N BURROWS, J E HILL, J A NOUSEK, J A KENNEA, A WELLS, J P OSBORNE, A F ABBEY, A BEARDMORE, K MUKERJEE, A D T SHORT, G CHINCARINI, S CAMPANA, O CITTERIO, A MORETTI, C PAGANI, G TAGLIAFERRI, P GIOMMI, M CAPALBI, F TAMBURELLI, L ANGELINI, G CUSUMANO, H W BRÄUNINGER, W BURKERT, AND G D HARTNER. **The Swift X-Ray Telescope**. *Space Science Reviews*, **120**(3-4):165–195, 2005. 52

[74] PETER W A ROMING, THOMAS E KENNEDY, KEITH O MASON, JOHN A NOUSEK, LINDY AHR, RICHARD E BINGHAM, PATRICK S BROOS, MARY J CARTER, BARRY K HANCOCK, HOWARD E HUCKLE, S D HUNSBERGER, HAJIME KAWAKAMI, RONNIE KILLOUGH, T SCOTT KOCH, MICHAEL K MCLELLAND, KELLY SMITH, PHILIP J SMITH, JUAN CARLOS SOTO, PATRICIA T BOYD, ALICE A BREEVELD, STEPHEN T HOLLAND, MARIYA IVANUSHKINA, MICHAEL S PRYZBY, MARTIN D STILL, AND JOSEPH STOCK. **The Swift Ultra-Violet/Optical Telescope**. *Space Science Reviews*, **120**(3-4):95–142, 2005. 52

[75] H L JOHNSON AND W W MORGAN. **Fundamental stellar photometry for standards of spectral type on the revised system of the Yerkes spectral atlas**. *The Astrophysical Journal*, **117**:313, 1953. 53

[76] JOCHEN GREINER, WALTER BORNEMANN, CHRISTIAN CLEMENS, MARTIN DEUTER, GÜNTHER HASINGER, MATHIAS HONSBERG, HEINRICH HUBER, STEFAN HUBER, MARKUS KRAUSS, THOMAS KRÜHLER, AYBÜKE KÜPCÜ YOLDAS, HANS MAYER-HASSELWANDER, BENJAMIN MICAN, NATALYA PRIMAK, FRITZ SCHREY, INGO STEINER, GYULA SZOKOLY, CHRISTINA C THÖNE, ABDULLAH YOLDAS, SYLVIO KLOSE, UWE LAUX, AND JOHANNES WINKLER. **GROND Commissioned at the 2.2-m MPI Telescopeon La Silla**. *The Messenger*, **130**:12–14, December 2007. 53

[77] J GREINER, W BORNEMANN, C CLEMENS, M DEUTER, G HASINGER, M HONSBERG, H HUBER, S HUBER, M KRAUSS, T KRÜHLER, A KÜPCÜ YOLDAŞ, H MAYER-HASSELWANDER, B MICAN, N PRIMAK, F SCHREY, I STEINER, G SZOKOLY, C C THÖNE, A YOLDAŞ, S KLOSE, U LAUX, AND J WINKLER. **GROND—a 7-Channel Imager**. *Publications of the Astronomical Society of the Pacific*, **120**(866):405–424, 2008. 53

[78] ZHANG, BING. **Gamma-Ray Bursts in the Swift Era**. *Chinese Journal of Astronomy and Astrophysics*, **7**(1):1–50, February 2007. 55

[79] BING ZHANG. **Open Questions in GRB Physics**. *arXiv.org*, pages 206–225, April 2011. 55

[80] J VAN PARADIJS, P J GROOT, T GALAMA, C KOUVELIOTOU, R G STROM, J TELTING, R G M RUTTEN, G J FISHMAN, C A MEEGAN, M PETTINI, N TANVIR, J BLOOM, H PEDERSEN, H U NØRDGAARD-NIELSEN, M LINDEN-VØRNLE, J MELNICK, G VAN DER STEENE, M BREMER, R NABER, J HEISE, J IN'T ZAND, E COSTA, M FEROCI, L PIRO, F FRONTERA, G ZAVATTINI, L NICASTRO, E PALAZZI, K BENNET, L HANLON, AND A PARMAR. **Transient optical emission from the error box of the γ-ray burst of 28 February 1997**. *Nature*, **386**(6626):686–689, 1997. 57

[81] ZEH, A, KLOSE, S, AND KANN, D A. **Gamma-Ray Burst Afterglow Light Curves in the Pre-Swift Era: A Statistical Study**. *The Astrophysical Journal*, **637**(2):889–900, February 2006. 57

[82] Y F HUANG, K S CHENG, AND T T GAO. **Modeling the Optical Afterglow of GRB 030329**. *The Astrophysical Journal*, **637**(2):873–879, 2006.

[83] KANN, D A, KLOSE, S, ZHANG, B, MALESANI, D, NAKAR, E, POZANENKO, A, WILSON, A C, BUTLER, N R, JAKOBSSON, P, SCHULZE, S, ANDREEV, M, ANTONELLI, L A, BIKMAEV, I F, BIRYUKOV, V, BÖTTCHER, M, BURENIN, R A, CASTRO CERÓN, J M, CASTRO-TIRADO, A J, CHINCARINI, G, COBB, B E, COVINO, S, D'AVANZO, P, D'ELIA, V, DELLA VALLE, M, DE UGARTE POSTIGO, A, EFIMOV, YU, FERRERO, P, FUGAZZA, D, FYNBO, J P U, GÅLFALK, M, GRUNDAHL, F, GOROSABEL, J, GUPTA, S, GUZIY, S, HAFIZOV, B, HJORTH, J, HOLHJEM, K, IBRAHIMOV, M, IM, M, ISRAEL, G L, JEĹINEK, M, JENSEN, B L, KARIMOV, R, KHAMITOV, I M, KIZILOĞLU, Ü, KLUNKO, E, KUBÁNEK, P, KUTYREV, A S, LAURSEN, P, LEVAN, A J, MANNUCCI, F, MARTIN, C M, MESCHERYAKOV, A, MIRABAL, N, NORRIS, J P, OVALDSEN, J E, PARAFICZ, D, PAVLENKO, E, PIRANOMONTE, S, ROSSI, A, RUMYANTSEV, V, SALINAS, R, SERGEEV, A, SHARAPOV, D, SOLLERMAN, J, STECKLUM, B, STELLA, L, TAGLIAFERRI, G, TANVIR, N R, TELTING, J, TESTA, V, UPDIKE, A C, VOLNOVA, A, WATSON, D, WIERSEMA, K, AND XU, D. **The Afterglows of Swift-era Gamma-ray Bursts. I. Comparing pre-Swift and Swift-era Long/Soft (Type II) GRB Optical Afterglows**. *The Astrophysical Journal*, **720**(2):1513–1558, September 2010. 57

[84] KANN, D A, KLOSE, S, ZHANG, B, COVINO, S, BUTLER, N R, MALESANI, D, NAKAR, E, WILSON, A C, ANTONELLI, L A, CHINCARINI, G, COBB, B E, D'AVANZO, P, D'ELIA, V, DELLA VALLE, M, FERRERO, P, FUGAZZA, D, GOROSABEL, J, ISRAEL, G L, MANNUCCI, F, PIRANOMONTE, S, SCHULZE, S, STELLA, L, TAGLIAFERRI, G, AND WIERSEMA, K. **THE AFTERGLOWS OF SWIFT-ERA GAMMA-RAY BURSTS. II. TYPE I GRB VERSUS TYPE II GRB OPTICAL AFTERGLOWS**. *The Astrophysical Journal*, **734**(2):96–47, June 2011.

[85] P. W. A. ROMING, T. S. KOCH, S. R. OATES, B. L. PORTERFIELD, A. J. BAYLESS, A. A. BREEVELD, C. GRONWALL, N. P. M. KUIN, M. J. PAGE, M. DE PASQUALE, M. H. SIEGEL, C. A. SWENSON, AND J. M. TOBLER. **A Large Catalog of Homogeneous Ultra-Violet/Optical GRB Afterglows: Temporal and Spectral Evolution**. *ArXiv e-prints*, January 2017. 57

[86] STRATTA, G, FIORE, F, ANTONELLI, L A, PIRO, L, AND DE PASQUALE, M. **Absorption in Gamma-Ray Burst Afterglows**. *The Astrophysical Journal*, **608**(2):846–864, June 2004.

[87] R L C STARLING, R A M J WIJERS, K WIERSEMA, E ROL, P A CURRAN, C KOUVELIOTOU, A J VAN DER HORST, AND M H M HEEMSKERK. **Gamma-Ray Burst Afterglows as Probes of Environment and Blast Wave Physics. I. Absorption by Host-Galaxy Gas and Dust**. *The Astrophysical Journal*, **661**(2):787–800, 2007. 57

[88] J A NOUSEK, C KOUVELIOTOU, D GRUPE, K L PAGE, J GRANOT, E RAMIREZ-RUIZ, S K PATEL, D N BURROWS, V MANGANO, S BARTHELMY, A P BEARDMORE, S CAMPANA, M CAPALBI, G CHINCARINI, G CUSUMANO, A D FALCONE, N GEHRELS, P GIOMMI, M R GOAD, O GODET, C P HURKETT, J A KENNEA, A MORETTI, P T O'BRIEN, J P OSBORNE, P ROMANO, G TAGLIAFERRI, AND A A WELLS. **Evidence for a Canonical Gamma-Ray Burst Afterglow Light Curve in the Swift XRT Data**. *The Astrophysical Journal*, **642**(1):389–400, May 2006. 61

[89] P T O'BRIEN, R WILLINGALE, J OSBORNE, M R GOAD, K L PAGE, S VAUGHAN, E ROL, A BEARDMORE, O GODET, C P HURKETT, A WELLS, B ZHANG, S KOBAYASHI, D N BURROWS, J A NOUSEK, J A KENNEA, A FALCONE, D GRUPE, N GEHRELS, S BARTHELMY, J CANNIZZO, J CUMMINGS, J E HILL, H KRIMM, G CHINCARINI, G TAGLIAFERRI, S CAMPANA, A MORETTI, P GIOMMI, M PERRI, V MANGANO, AND V LAPAROLA. **The Early X-Ray Emission from GRBs**. *The Astrophysical Journal*, **647**(2):1213–1237, August 2006. 61

[90] PAWAN KUMAR AND TSVI PIRAN. **Some Observational Consequences of Gamma-Ray Burst Shock Models**. *The Astrophysical Journal*, **532**(1):286–293, March 2000. 61

[91] BING ZHANG AND PETER MÉSZÁROS. **Gamma-Ray Bursts with Continuous Energy Injection and Their Afterglow Signature**. *The Astrophysical Journal*, **566**(2):712–722, February 2002.

[92] Z G DAI. **Relativistic Wind Bubbles and Afterglow Signatures**. *The Astrophysical Journal*, **606**(2):1000–1005, May 2004.

[93] JONATHAN GRANOT AND PAWAN KUMAR. **Distribution of gamma-ray burst ejecta energy with Lorentz factor**. *Monthly Notices of the Royal Astronomical Society: Letters*, **366**(1):L13–L16, February 2006.

[94] A PANAITESCU, P MÉSZÁROS, N GEHRELS, D BURROWS, AND J NOUSEK. **Analysis of the X-ray emission of nine Swift afterglows**. *Monthly Notices of the Royal Astronomical Society*, **366**(4):1357–1366, March 2006. 61